# The effect of interfaces on the plastic behavior of periodic composites

Martin Ignacio Idiart, Norman Fleck


# The effect of interfaces on the plastic behavior of periodic composites

| | |
|---|---|
| Journal: | *Philosophical Magazine & Philosophical Magazine Letters* |
| Manuscript ID: | TPHM-07-Dec-0384.R1 |
| Journal Selection: | Philosophical Magazine |
| Date Submitted by the Author: | 20-Feb-2008 |
| Complete List of Authors: | Idiart, Martin; University of Cambridge, Department of Engineering<br>Fleck, Norman; University of Cambridge, Department of Engineering |
| Keywords: | composite materials, interfaces, mechanical properties |
| Keywords (user supplied): | composite materials, interfaces, mechanical properties |
| | |
| Note: The following files were submitted by the author for peer review, but cannot be converted to PDF. You must view these files (e.g. movies) online. | |
| Idiart-Fleck-2008.tex | |


# The effect of interfaces on the plastic behavior of periodic composites

| | |
|---|---|
| Journal: | *Philosophical Magazine & Philosophical Magazine Letters* |
| Manuscript ID: | TPHM-07-Dec-0384.R1 |
| Journal Selection: | Philosophical Magazine |
| Date Submitted by the Author: | 20-Feb-2008 |
| Complete List of Authors: | Idiart, Martin; University of Cambridge, Department of Engineering<br>Fleck, Norman; University of Cambridge, Department of Engineering |
| Keywords: | composite materials, interfaces, mechanical properties |
| Keywords (user supplied): | composite materials, interfaces, mechanical properties |
| | |

*Philosophical Magazine*,
Vol. 00, No. 00, DD Month 200x, 1–19

# The effect of interfaces on the plastic behavior of periodic composites

M.I. Idiart*, N.A. Fleck,

Centre for Micromechanics, Cambridge University Engineering Department,
Trumpington Street, Cambridge CB2 1PZ, U.K.

*(February 20, 2008)*

A theoretical framework is given for predicting the effect of microstructural size on the strength of $N$-phase periodic composites. It is assumed that the strength is elevated by plastic strain gradients in the bulk and by the resistance to plastic slip at internal material interfaces. Calculations are given for a two-phase, power-law material with a cubic array of spherical reinforcement particles. The macroscopic stress-strain relations are found to exhibit Hall-Petch behavior, and the size effect becomes more pronounced with increasing interface strength. Moreover, size effects are predicted for both yield strength and plastic hardening rate of the composite. The relative magnitude of these two effects is sensitive to the choice of constitutive description of the interface.

## 1 Introduction: two-phase nanocrystalline materials

As the microstructure of a metallic composite becomes finer, the strength can be significantly elevated due to the slip resistance of internal interfaces. Examples include the well-known Hall-Petch size effect in polycrystals, and the size effects observed in reinforced metal-matrix composites [1, 2] and nanoscale metallic laminates [3].

A macro-hardness test is commonly used to measure the plastic strength of a composite. For example, He and Ma [4] report that the hardness of an Fe-Cu nanocrystalline composite is significantly above the hardness of a coarse-grained composite of identical composition. These nanophase composites comprised intimately mixed Fe-rich grains and Cu-rich grains, with relatively low clustering of each phase. Figure 1a shows the Vickers hardness $HV$ values reported by these authors for Fe-Cu systems with mean grain sizes close to 40nm, as a function of Fe volume fraction. The measured values lie consistently above the rule of mixtures based on the elementary nanocrystalline phases. This suggests that the strength of these two-phase materials ($\sigma_0 \approx HV/3$) is larger than the classical Voigt upper bound derived from conventional plasticity theory. He and Ma [4, 5] conjectured that Fe-Cu (bcc-fcc) interfaces, or interphases, should be more effective in impeding plastic slip than their Fe-Fe (bcc-bcc) and Cu-Cu (fcc-fcc) counterparts, and attempted to modify the rule of mixtures by treating interphases as a third phase.

The homogenization of nonlinear composites has been extensively treated during the last twenty years –see, for instance, the review articles by Ponte Castañeda and Suquet [6] and Willis [7]–. However, this literature deals almost exclusively with standard plasticity theories. More recently, strain gradient plasticity theories have been used to predict size effects in composites and polycrystals (*e.g.*, [8–11]), but with no explicit model of the interface between constituent phases or grains. An extended framework which accounts for strain-gradient and interface effects on the plastic response of composites has been recently proposed by Aifantis and Willis [12] (see also, Gurtin and Anand [13]). They employed the framework of Fleck and Willis [10] and enhanced it by the introduction of an interfacial 'energy' term that penalizes the accumulation of plastic strain at interfaces. One of the most notable features of this augmented framework is that the predictions for the effective response of composite materials are no longer limited by the classical Voigt bound. Instead, a new Voigt-type upper bound was derived which is elevated by the interfacial term and increases linearly with the surface area-to-volume ratio of the internal interfaces. To motivate the main contents of the paper, this new Voigt bound is applied to a two-phase composite in order to derive

*Corresponding author. Email: mii23@cam.ac.uk

*Philosophical Magazine*
ISSN 1478-6435 print/ISSN 1478-6443 online © 200x Taylor & Francis
http://www.tandf.co.uk/journals
DOI: 10.1080/1478643YYxxxxxxxx

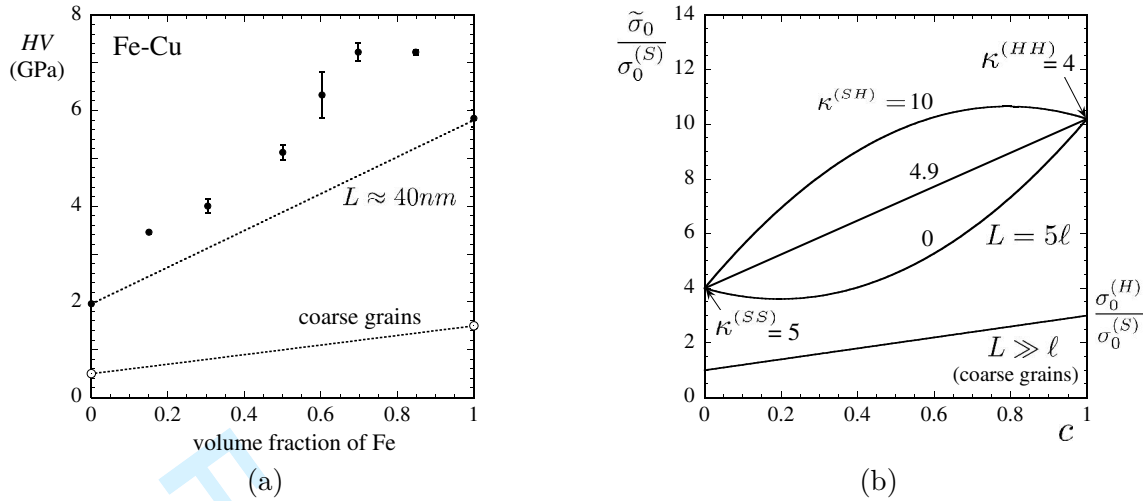


Figure 1. (a) Vickers hardness of Fe-Cu nanocrystalline composites ($L \approx 40$nm) versus the volume fraction of Fe, from [4]. (b) Elementary Voigt bounds for the effective strength of a two-phase composite with interfaces, as a function of volume fraction $c$ of the hard phase.

a modified rule of mixtures. The body of the paper then deals with the derivation of refined bounds and estimates for the elastoplastic response of more general, $N$-phase periodic composites with internal interfaces.

Two-phase nanocrystalline materials are idealized here as *random* assemblages of 'hard' ($H$) and 'soft' ($S$) cubic grains of side length $L$, as shown in Table 1. Let $c^{(H)} = c$ and $c^{(S)} = (1-c)$ denote the volume fractions of the hard and soft phases, respectively, and let $p^{(HH)}$, $p^{(SS)}$ and $p^{(SH)}$ denote the surface area-to-volume ratios of each of the three possible types of interfaces: hard-hard ($HH$), soft-soft ($SS$), and soft-hard ($SH$). The behavior of the grains is assumed to be isotropic and elastic-perfectly plastic, with uniaxial strengths $\sigma_0^{(H)}$ and $\sigma_0^{(S)}$, while the interfaces are assumed to be isotropic and 'rigid-perfectly plastic' as in [12], with 'strengths' $\tau_0^{(HH)}$, $\tau_0^{(SS)}$ and $\tau_0^{(SH)}$. These interface strengths have dimensions of length×stress, and can be written in the non-dimensional form $\kappa^{(rs)} = \tau_0^{(rs)} / \left[\ell(\sigma_0^{(r)}\sigma_0^{(s)})^{1/2}\right]$ $(r, s = H, S)$, where $\ell$ is a material length scale. The macroscopic response of the aggregate is isotropic and elastic-perfectly plastic. Let $\widetilde{\sigma}_0$ denote its uniaxial effective strength. The Voigt bound of Aifantis and Willis (expression (4.5) in [12]) then gives

$$\widetilde{\sigma}_0 = c^{(S)}\sigma_0^{(S)} + c^{(H)}\sigma_0^{(H)} + p^{(SS)}\tau_0^{(SS)} + p^{(HH)}\tau_0^{(HH)} + p^{(SH)}\tau_0^{(SH)}. \tag{1}$$

It is clear from this expression that the surface area-to-volume ratios must be specified. To that end, we make the following assumptions: i) the microstructure is ergodic, ii) the probability for a given grain being hard (resp. soft) is given by the volume fraction $c$ (resp. $1-c$), iii) the grains are uncorrelated. The last assumption is justified by the assertion that the phases are intimately mixed. These assumptions allow us to compute the probabilities of a given interface being either of the $SS$, $HH$, or $SH$ type, and identify those probabilities with the corresponding surface fractions. Thus, the probability of a given interface being of type $rs$ equals the probability of the two adjacent grains being of type $r$ and $s$ simultaneously. By assumptions ii and iii, this probability equals the product of the volume fractions $c^{(r)}c^{(s)}$. It can then be shown that the resulting surface area-to-volume ratios are given by $p^{(rs)} = (3/L)c^{(r)}c^{(s)}(2-\delta_{rs})$, where the factor $3/L$ corresponds to the total surface area-to-volume ratio associated with an array of cubes. The characteristics of each component are summerized in Table 1. Thus, the Voigt bound (1) becomes

$$\widetilde{\sigma}_0 = (1-c)\sigma_0^{(S)} + c\,\sigma_0^{(H)} + 3\frac{\ell}{L}\left[(1-c)^2\,\kappa^{(SS)}\sigma_0^{(S)} + c^2\,\kappa^{(HH)}\sigma_0^{(H)} + 2c(1-c)\,\kappa^{(SH)}\left(\sigma_0^{(H)}\sigma_0^{(S)}\right)^{1/2}\right], \tag{2}$$

where the volume fraction $c$ of the hard phase and the grain size $L$ are the only microstructural parameters

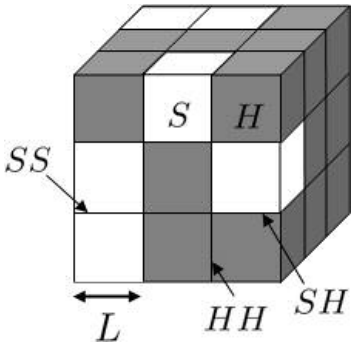


| component | strength | vol. fraction or surf./vol. ratio |
|---|---|---|
| hard phase | $\sigma_0^{(H)}$ | $c$ |
| soft phase | $\sigma_0^{(S)}$ | $1-c$ |
| hard-hard interfaces | $\kappa^{(HH)}\ell\sigma_0^{(H)}$ | $(3/L)\ c^2$ |
| soft-soft interfaces | $\kappa^{(SS)}\ell\sigma_0^{(S)}$ | $(3/L)(1-c)^2$ |
| hard-soft interfaces | $\kappa^{(SH)}\ell\left(\sigma_0^{(S)}\sigma_0^{(H)}\right)^{1/2}$ | $(3/L)\ 2c(1-c)$ |

Table 1. Idealized two-phase nanocrystalline material with interfaces.

required. For coarse-grained composites ($L \gg \ell$), the contribution of the interfacial terms to the effective strength is negligible, and the bound reduces to the standard rule of mixtures. On the other hand, when the grain size $L$ is comparable to the length scale $\ell$, the bound can be significantly elevated as a result of interface strengthening. Figure 1b illustrates this for the choice $\sigma_0^{(H)}/\sigma_0^{(S)} = 3$, $\kappa^{(HH)} = 4$, $\kappa^{(SS)} = 5$, and three different values of $\kappa^{(SH)}$ $(0, 4.9, 10)$. When the $SH$ interfaces are sufficiently strong relative to the $HH$ and $SS$ interfaces, the bound lies well above the rule of mixtures based on the fine-grained constituents, in agreement with the trend exhibited by the experimental results shown in fig. 1a. For lower values of $\kappa^{(SH)}$, the bound may coincide with the fine-grained rule of mixtures and even lie below it. In summary, by introducing interface strengthening in the manner proposed in [12], a simple, modified rule of mixtures has been derived that may give predictions above the standard rule of mixtures and can reproduce, at least qualitatively, the dependence of strength on volume fractions observed in the two-phase nanocrystalline materials of fig. 1a.

The enhanced Voigt bound makes use of first-order statistical information of the microstructure, namely, volume fractions and surface area-to-volume ratios only. More accurate predictions for *random* composites require higher-order statistics, such as the two-point correlation functions of the microstructure. In addition to volume-volume correlations, the introduction of interfaces in the formulation induces the need to determine consistent surface-surface and surface-volume correlations. So far, this has only been achieved in the context of certain one-dimensional examples [12, 14]. The strategy adopted in the reminder of this study is to consider deterministic periodic microstructures. Consequently, the estimation of the effective properties reduces to a unit cell calculation. Simple, semi-analytical models are developed for the non-linear response of 3D composites, including strain-gradient and interface effects. An alternative approach would be to perform finite element calculations using non-standard techniques (*e.g.*, [9,11]). However, this alternative approach is much more intensive computationally, and is not pursued further here.

The study begins with an outline of the strain-gradient plasticity framework proposed by Fleck and Willis [10], as modified by Aifantis and Willis [12] to include interface effects. The framework is used to express the effective response of a periodic composite with interfaces in terms of an effective potential. Bounds and estimates for the effective potential are then derived by means of a variational procedure first introduced by Ponte Castañeda [15] for conventional elastoplastic composites. The procedure requires the effective properties of a 'linear comparison composite' with periodic microstructure. These properties are obtained by following the strategy first laid down by Hashin and Shtrikman [16] and applied to periodic elastic composites by Nemat-Nasser *et al.* [17] and Suquet [18]. As an illustrative example, estimates are computed for particle-reinforced power-law composites, and the influence of interface constitutive description on the effective response is explored.

## 2 Periodic composites with interfaces: strain-gradient plasticity framework

We begin by summerizing the deformation theory of strain-gradient plasticity as proposed by Fleck and Willis [10] and as modified by Aifantis and Willis [12] to include interface effects. An expression is obtained

for the relevant potential that describes the effective response of periodic composites. Consider a material occupying a domain $\Omega$ and composed of different homogeneous phases. The boundaries between the phases form internal interfaces that are collectively denoted by $\Gamma$. The displacement $\mathbf{u}$ and plastic strain $\boldsymbol{\varepsilon}^p$ fields are taken as *independent* kinematical variables. Now introduce the variational statement [12]

$$\Psi = \inf_{(\boldsymbol{\varepsilon},\boldsymbol{\varepsilon}^p)\in\mathcal{K}} \left\{ \int_\Omega w(\mathbf{x},\boldsymbol{\varepsilon},\boldsymbol{\varepsilon}^p,\nabla\boldsymbol{\varepsilon}^p)\ d\Omega + \int_\Gamma \phi(\mathbf{x},\boldsymbol{\varepsilon}^p)\ d\Gamma \right\}, \tag{3}$$

where $w$ and $\phi$ are, respectively, bulk and interface strain energy densities, and $\mathcal{K}$ denotes the set of kinematically admissible fields, such that the total strain $\boldsymbol{\varepsilon} = \mathrm{sym}\,(\nabla\mathbf{u})$ in $\Omega$ and $\mathbf{u} = \mathbf{u}^0$ on the surface $\partial\Omega$, with $\mathbf{u}$ and $\boldsymbol{\varepsilon}^p$ continuous throughout the domain. The elasto-plastic potential $w$ is defined as [10]

$$w(\mathbf{x},\boldsymbol{\varepsilon},\boldsymbol{\varepsilon}^p,\boldsymbol{\eta}^p) = \frac{1}{2}\,(\boldsymbol{\varepsilon}-\boldsymbol{\varepsilon}^p)\cdot\mathbf{L}\,(\boldsymbol{\varepsilon}-\boldsymbol{\varepsilon}^p) + V(\mathbf{x},\boldsymbol{\varepsilon}^p,\boldsymbol{\eta}^p), \tag{4}$$

where $\mathbf{L}$ is the elasticity tensor, and $V$ is a plastic potential that depends on the plastic strain and its gradient $\boldsymbol{\eta}^p \equiv \nabla\boldsymbol{\varepsilon}^p$. Thus, a material length scale enters naturally on dimensional grounds. The present development considers small displacements and strains, and the functions $V(\mathbf{x},\cdot,\cdot)$ and $\phi(\mathbf{x},\cdot)$ are assumed to be *convex*.

The presence of plastic strain gradients in the constitutive law accounts phenomenologically for the effect of geometrically necessary dislocations on bulk material hardening (see, for instance, Fleck and Hutchinson [19]), while the introduction of an interfacial 'energy' term, penalizing the accumulation of plastic strain there, follows from the accepted notion that interfaces represent an obstruction to the motion of dislocations. Recent attempts to determine the interface potential $\phi$ experimentally include nanoindentation tests in the vicinity of grain boundaries [20], and tensile tests on bicrystals [21]. Additionally, atomistic simulations of dislocation/grain-boundary interactions [22] should prove useful in determining this potential.

Equilibrium equations are obtained by setting the first variation of (3) equal to zero, giving

$$\left.\begin{aligned} \nabla\cdot\boldsymbol{\sigma} &= \mathbf{0} \\ \mathbf{s} - \nabla\cdot\boldsymbol{\tau} &= \mathbf{0} \end{aligned}\right\} \text{ in } \Omega\backslash\Gamma, \qquad \left.\begin{aligned} [\boldsymbol{\sigma}\mathbf{n}] &= \mathbf{0} \\ [\boldsymbol{\tau}\mathbf{n}] &= \frac{\partial\phi}{\partial\boldsymbol{\varepsilon}^p}(\boldsymbol{\varepsilon}^p) \end{aligned}\right\} \text{ across } \Gamma, \tag{5}$$

in terms of the usual Cauchy stress $\boldsymbol{\sigma}$, a back stress $\mathbf{s}$, and a hyperstress $\boldsymbol{\tau}$, each defined as

$$\boldsymbol{\sigma} = \frac{\partial w}{\partial\boldsymbol{\varepsilon}} = \mathbf{L}(\boldsymbol{\varepsilon}-\boldsymbol{\varepsilon}^p), \quad \mathbf{s} = \frac{\partial w}{\partial\boldsymbol{\varepsilon}^p} = -\mathbf{L}(\boldsymbol{\varepsilon}-\boldsymbol{\varepsilon}^p) + \frac{\partial V}{\partial\boldsymbol{\varepsilon}^p}, \quad \boldsymbol{\tau} = \frac{\partial w}{\partial\boldsymbol{\eta}^p} = \frac{\partial V}{\partial\boldsymbol{\eta}^p}. \tag{6}$$

In expressions (5), $[\cdot]$ denotes the jump across a point on $\Gamma$ with normal $\mathbf{n}$. The Fleck-Willis formulation [10] is recovered by setting $\phi \equiv 0$.

The interest here is on composite materials whose phases are *periodically* distributed on a length scale which is intermediate between the internal material length scale and the typical size of a specimen. Let $\Omega_\#$ denote the domain of the unit cell, and $\Gamma_\#$ the set of internal interfaces within it. As argued by Aifantis and Willis [12], the problem (3) can then be replaced asymptotically by the homogenized problem

$$\Psi = \inf_{(\overline{\boldsymbol{\varepsilon}},\overline{\boldsymbol{\varepsilon}}^p)\in\mathcal{K}} \int_\Omega \widetilde{W}(\overline{\boldsymbol{\varepsilon}},\overline{\boldsymbol{\varepsilon}}^p)\ d\Omega, \tag{7}$$

where $\widetilde{W}$ is an *effective strain potential* defined by

$$\widetilde{W}(\overline{\boldsymbol{\varepsilon}},\overline{\boldsymbol{\varepsilon}}^p) = \inf_{(\boldsymbol{\varepsilon}',\boldsymbol{\varepsilon}^{p\prime})\in\mathcal{K}_\#} \frac{1}{\Omega_\#} \left\{ \int_{\Omega_\#} w(\mathbf{x},\overline{\boldsymbol{\varepsilon}}+\boldsymbol{\varepsilon}',\overline{\boldsymbol{\varepsilon}}^p+\boldsymbol{\varepsilon}^{p\prime},\nabla\boldsymbol{\varepsilon}^{p\prime})\ d\Omega + \int_{\Gamma_\#} \phi(\mathbf{x},\overline{\boldsymbol{\varepsilon}}^p+\boldsymbol{\varepsilon}^{p\prime})\ d\Gamma \right\}. \tag{8}$$

In this expression, $\mathcal{K}_\#$ is the set of kinematically admissible periodic fields with period $\Omega_\#$ and zero mean. Define $\overline{\boldsymbol{\sigma}}$ as the mean value of $\boldsymbol{\sigma}$ over the unit cell. Then, consideration of the variation in (7) with respect to the macroscopic fields delivers the *effective response* of the composite in the form [12]

$$\overline{\boldsymbol{\sigma}} = \frac{\partial \widetilde{W}}{\partial \overline{\boldsymbol{\varepsilon}}}(\overline{\boldsymbol{\varepsilon}}, \overline{\boldsymbol{\varepsilon}}^p), \quad \text{with } \overline{\boldsymbol{\varepsilon}}^p \text{ satisfying the condition } \quad \frac{\partial \widetilde{W}}{\partial \overline{\boldsymbol{\varepsilon}}^p}(\overline{\boldsymbol{\varepsilon}}, \overline{\boldsymbol{\varepsilon}}^p) = \mathbf{0}. \tag{9}$$

For simplicity, we specialize to the case where the elasticity tensor $\mathbf{L}$ in (4) is spatially *uniform*. The potential (8) then reduces to [10, 12]

$$\widetilde{W}(\overline{\boldsymbol{\varepsilon}}, \overline{\boldsymbol{\varepsilon}}^p) = \frac{1}{2}\,(\overline{\boldsymbol{\varepsilon}} - \overline{\boldsymbol{\varepsilon}}^p) \cdot \mathbf{L}\,(\overline{\boldsymbol{\varepsilon}} - \overline{\boldsymbol{\varepsilon}}^p) + \widetilde{V}(\overline{\boldsymbol{\varepsilon}}^p), \tag{10}$$

where $\widetilde{V}$ is an *effective plastic potential*, given by

$$\widetilde{V}(\overline{\boldsymbol{\varepsilon}}^p) = \inf_{(\boldsymbol{\varepsilon}', \boldsymbol{\varepsilon}^{p'}) \in \mathcal{K}_\#} \frac{1}{\Omega_\#} \left\{ \int_{\Omega_\#} \left( \frac{1}{2}(\boldsymbol{\varepsilon}' - \boldsymbol{\varepsilon}^{p'}) \cdot \mathbf{L}(\boldsymbol{\varepsilon}' - \boldsymbol{\varepsilon}^{p'}) + V(\mathbf{x}, \overline{\boldsymbol{\varepsilon}}^p + \boldsymbol{\varepsilon}^{p'}, \nabla \boldsymbol{\varepsilon}^{p'}) \right) d\Omega \right.$$
$$\left. + \int_{\Gamma_\#} \phi(\mathbf{x}, \overline{\boldsymbol{\varepsilon}}^p + \boldsymbol{\varepsilon}^{p'})\, d\Gamma \right\}. \tag{11}$$

The effective plastic response of the composite follows from (9) and (10) as

$$\overline{\boldsymbol{\sigma}} = \frac{\partial \widetilde{V}}{\partial \overline{\boldsymbol{\varepsilon}}^p}(\overline{\boldsymbol{\varepsilon}}^p). \tag{12}$$

Thus, the effective response of the composite requires computing the effective plastic potential defined by (11). Simple bounds and estimates for this potential are derived below.

Once the effective potential $\widetilde{V}$ is known, the effective strain follows as

$$\overline{\boldsymbol{\varepsilon}} = \mathbf{L}^{-1}\overline{\boldsymbol{\sigma}} + \frac{\partial \widetilde{V}^*}{\partial \overline{\boldsymbol{\sigma}}}(\overline{\boldsymbol{\sigma}}), \tag{13}$$

where $\widetilde{V}^*$ is the Legendre-Fenchel transform (or convex polar) of $\widetilde{V}$, defined as

$$\widetilde{V}^*(\overline{\boldsymbol{\sigma}}) = \sup_{\overline{\boldsymbol{\varepsilon}}^p} \left[ \overline{\boldsymbol{\sigma}} \cdot \overline{\boldsymbol{\varepsilon}}^p - \widetilde{V}(\overline{\boldsymbol{\varepsilon}}^p) \right]. \tag{14}$$

## 3 Bounds and estimates for $\widetilde{V}$

Let $N$ denote the number of distinct types of phase making up the composite, and let $M$ denote the number of types of internal interface between these phases. The plastic potential $V$ and interface potential $\phi$ can then be written as

$$V(\mathbf{x}, \boldsymbol{\varepsilon}^p, \boldsymbol{\eta}^p) = \sum_{r=1}^{N} \chi_\Omega^{(r)}(\mathbf{x})\; V^{(r)}(\boldsymbol{\varepsilon}^p, \boldsymbol{\eta}^p), \quad \phi(\mathbf{x}, \boldsymbol{\varepsilon}^p) = \sum_{i=1}^{M} \chi_\Gamma^{(i)}(\mathbf{x})\; \phi^{(i)}(\boldsymbol{\varepsilon}^p), \tag{15}$$

where $V^{(r)}$ and $\phi^{(i)}$ denote the potentials of phase $r$ and interface $i$, respectively. The volumetric distribution of the phases is described by the periodic characteristic functions $\chi_\Omega^{(r)}(\mathbf{x})$, which take the value 1 if $\mathbf{x}$ is in phase $r$, and zero otherwise, while the distribution of the interfaces is described by the periodic

functions $\chi_\Gamma^{(i)}(\mathbf{x})$, defined in a similar fashion. In contrast with the explicit but lengthy notation of Section 1, interfaces are labelled here with one index only in order to give compact notations in the calculations carried out in Section 3.3.

### 3.1 *Elementary bounds of the Voigt and Reuss type*

Elementary bounds of the Voigt and Reuss type have been derived by Aifantis and Willis [12], and are recalled here for completeness. These bounds are expressed in terms of the volume fraction $c^{(r)}$ of each phase $r$, and of the surface area per unit volume of composite, denoted by $p^{(i)}$, of interface type $i$.

The Voigt *upper* bound is obtained by letting the local strain fields in (11) be uniform and equal to the corresponding macroscopic quantities, *i.e.*, $\boldsymbol{\varepsilon}' = \boldsymbol{\varepsilon}^{p'} = \mathbf{0}$, what yields

$$\widetilde{V}(\overline{\boldsymbol{\varepsilon}}^p) \leq \sum_{r=1}^{N} c^{(r)} V^{(r)}(\overline{\boldsymbol{\varepsilon}}^p, \mathbf{0}) + \sum_{i=1}^{M} p^{(i)} \phi^{(i)}(\overline{\boldsymbol{\varepsilon}}^p). \tag{16}$$

This bound incorporates limited microstructural information through the $c^{(r)}$ and $p^{(i)}$ only, and is independent of the elasticity tensor $\mathbf{L}$. However, it does depend on the interface potentials and on the microstructural size.

The Reuss *lower* bound is obtained by assuming a uniform stress field in the dual formulation to (11), and is stated by

$$\widetilde{V}(\overline{\boldsymbol{\varepsilon}}^p) \geq \sup_{\overline{\boldsymbol{\sigma}}} \left[ \overline{\boldsymbol{\sigma}} \cdot \overline{\boldsymbol{\varepsilon}}^p - \sum_{r=1}^{N} c^{(r)} (V^{(r)})^*(\overline{\boldsymbol{\sigma}}, \mathbf{0}) \right]. \tag{17}$$

We emphasize that this bound is insensitive to the presence of interfaces, and exhibits no size effects.

### 3.2 *Nonlinear bounds and estimates using a 'linear comparison composite'*

Following a variational procedure as first introduced by Ponte Castañeda [15] for standard plastic solids, Aifantis and Willis [12] have derived refined bounds and estimates which incorporate information about the microstructure beyond the volume fractions and surface area-to-volume ratios, and can improve significantly on the above elementary bounds. The central idea behind this procedure is the introduction of a fictitious 'linear comparison composite' (LCC) with the same microstructure as that of the nonlinear composite, but with phases and interfaces characterized by quadratic potentials of the form

$$V_L^{(r)}(\boldsymbol{\varepsilon}^p, \boldsymbol{\eta}^p) = \frac{1}{2} \boldsymbol{\varepsilon}^p \cdot \mathbf{M}^{(r)} \boldsymbol{\varepsilon}^p + \frac{1}{2} \boldsymbol{\eta}^p \cdot \mathbf{N}^{(r)} \boldsymbol{\eta}^p, \tag{18}$$

$$\phi_L^{(i)}(\boldsymbol{\varepsilon}^p) = \frac{1}{2} \boldsymbol{\varepsilon}^p \cdot \mathbf{S}^{(i)} \boldsymbol{\varepsilon}^p, \tag{19}$$

where the modulus tensors $\mathbf{M}^{(r)}$, $\mathbf{N}^{(r)}$ and $\mathbf{S}^{(i)}$ are positive definite. Assume that the nonlinearity of the potentials $V^{(r)}$ and $\phi^{(i)}$ is weaker than quadratic: this is generally the case for rate-independent plasticity. With this restriction, $\widetilde{V}$ is bounded from above by [12]

$$\widetilde{V}(\overline{\boldsymbol{\varepsilon}}^p) \leq \inf_{\mathbf{M}^{(r)}, \mathbf{N}^{(r)}, \mathbf{S}^{(i)}} \left\{ \widetilde{V}_L(\overline{\boldsymbol{\varepsilon}}^p; \mathbf{M}^{(r)}, \mathbf{N}^{(r)}, \mathbf{S}^{(i)}) + \sum_{r=1}^{N} c^{(r)} v_\Omega^{(r)}(\mathbf{M}^{(r)}, \mathbf{N}^{(r)}) + \sum_{i=1}^{M} p^{(i)} v_\Gamma^{(i)}(\mathbf{S}^{(i)}) \right\}, \tag{20}$$

in terms of the effective potential $\widetilde{V}_L$ of the LCC, and of the 'corrector' functions

$$v_\Omega^{(r)}(\mathbf{M}^{(r)},\mathbf{N}^{(r)}) = \sup_{\boldsymbol{\varepsilon}^{(r)},\boldsymbol{\eta}^{(r)}} \left[V^{(r)}(\boldsymbol{\varepsilon}^{(r)},\boldsymbol{\eta}^{(r)}) - V_L^{(r)}(\boldsymbol{\varepsilon}^{(r)},\boldsymbol{\eta}^{(r)})\right], \tag{21}$$

$$v_\Gamma^{(i)}(\mathbf{S}^{(i)}) = \sup_{\boldsymbol{\varepsilon}^{(i)}} \left[\phi^{(i)}(\boldsymbol{\varepsilon}^{(i)}) - \phi_L^{(i)}(\boldsymbol{\varepsilon}^{(i)})\right]. \tag{22}$$

Thus, the problem of bounding the nonlinear potential $\widetilde{V}$ is reduced to two simpler problems, namely, bounding a linear potential $\widetilde{V}_L$, and optimizing with respect to the properties of the LCC. Expression (20) is an upper bound for $\widetilde{V}$ provided $\widetilde{V}_L$ is computed exactly or bounded from above. On the other hand, if use is made of an estimate or lower bound for $\widetilde{V}_L$, then expression (20) yields a variational estimate for $\widetilde{V}$.

The Euler-Lagrange equations associated with the effective potential $\widetilde{V}_L$ are linear. It then follows that $\widetilde{V}_L$ is of the form

$$\widetilde{V}_L(\overline{\boldsymbol{\varepsilon}}^p) = \frac{1}{2}\overline{\boldsymbol{\varepsilon}}^p \cdot \widetilde{\mathbf{M}}\overline{\boldsymbol{\varepsilon}}^p, \tag{23}$$

where $\widetilde{\mathbf{M}}$ is an effective plastic modulus that depends on the tensors $\mathbf{M}^{(r)}$, $\mathbf{N}^{(r)}$, $\mathbf{S}^{(i)}$ and the microstructure (see below).

In the case of anisotropic potentials $V^{(r)}$ and $\phi$, the 'corrector' functions (21) and (22) may be difficult to compute, for they require the solution to a non-convex optimization problem in a multi-dimensional unbounded space. However, their computation becomes straightforward in the case of isotropic potentials such as those considered in Section 4. In any event, the functions that result from the optimizations (21)-(22) are convex in the tensors $\mathbf{M}^{(r)}$, $\mathbf{N}^{(r)}$, $\mathbf{S}^{(i)}$, so that the minimization in (20) can be carried out using any standard method for convex optimization.

**3.2.1** ***Effective response and average plastic strains.*** An estimate for the effective response of the composite can be obtained by differentiating (20), in accordance with (12). By following similar arguments to those of [23], it can be shown that

$$\overline{\boldsymbol{\sigma}} = \frac{\partial \widetilde{V}}{\partial \overline{\boldsymbol{\varepsilon}}^p}(\overline{\boldsymbol{\varepsilon}}^p) = \frac{\partial \widetilde{V}_L}{\partial \overline{\boldsymbol{\varepsilon}}^p}(\overline{\boldsymbol{\varepsilon}}^p) = \widetilde{\mathbf{M}}\overline{\boldsymbol{\varepsilon}}^p, \tag{24}$$

where $\widetilde{\mathbf{M}}$ is evaluated at the optimal modulus tensors. This result avoids the complication of having to differentiate expression (20) numerically.

In addition to estimating the effective response, it is of interest to estimate the statistics of the plastic strain field. Following arguments given in [24], it can be shown that the nonlinear estimates for the average plastic strain in each phase and on each set of interfaces are given by the corresponding averages in the LCC (see below).

### 3.3 *Linear bounds and estimates for periodic composites*

The variational procedure given in the previous subsection requires an expression for the effective potential $\widetilde{V}_L$ of the relevant LCC. In this subsection, bounds and estimates for $\widetilde{V}_L$ are derived following the strategy for conventional linear composites laid down by Hashin and Shtrikman [16] and developed further by Willis [25]. In the context of periodic composites, this strategy has been introduced by Nemat-Nasser *et al.* [17] and given a more general form by Suquet [18]. Generalizations to linear composites with gradient effects have been given by Smyshlyaev and Fleck [26,27], Fleck and Willis [10], and Aifantis and Willis [14].

**3.3.1** ***Hashin-Shtrikman lower bound.*** Introduce a linear reference solid which is homogeneous in properties. The solid is characterized by a potential of the form (4), but with a plastic potential

$$V_0(\boldsymbol{\varepsilon}^p, \boldsymbol{\eta}^p) = \frac{1}{2}\boldsymbol{\varepsilon}^p \cdot \mathbf{M}^{(0)}\boldsymbol{\varepsilon}^p + \boldsymbol{\eta}^p \cdot \mathbf{N}^{(0)}\boldsymbol{\eta}^p, \tag{25}$$

where $\mathbf{M}^{(0)}$ and $\mathbf{N}^{(0)}$ must be chosen so that the tensors $(\mathbf{M}^{(r)} - \mathbf{M}^{(0)})$ and $(\mathbf{N}^{(r)} - \mathbf{N}^{(0)})$ are positive definite for all $r$. Define the functions $V_L$ and $\phi_L$ in terms of the potentials $V_L^{(r)}$ and $\phi_L^{(i)}$ by expressions analogous to (15), and consider the Legendre-Fenchel transforms

$$(V_L - V_0)^*(\mathbf{x}, \boldsymbol{\tau}, \mathbf{t}) = \sup_{\boldsymbol{\varepsilon}^p,\, \boldsymbol{\eta}^p} \left[\boldsymbol{\tau} \cdot \boldsymbol{\varepsilon}^p + \mathbf{t} \cdot \boldsymbol{\eta}^p - (V_L - V_0)(\mathbf{x}, \boldsymbol{\varepsilon}^p, \boldsymbol{\eta}^p)\right], \tag{26}$$

$$(\phi_L)^*(\mathbf{x}, \boldsymbol{\rho}) = \sup_{\boldsymbol{\varepsilon}^p} \left[\boldsymbol{\rho} \cdot \boldsymbol{\varepsilon}^p - \phi_L(\mathbf{x}, \boldsymbol{\varepsilon}^p)\right]. \tag{27}$$

Since the functions $(V_L - V_0)$ and $\phi_L$ are *convex* in $\boldsymbol{\varepsilon}^p$ and $\boldsymbol{\eta}^p$, they can be expressed in terms of their Legendre-Fenchel transforms as

$$(V_L - V_0)(\mathbf{x}, \boldsymbol{\varepsilon}^p, \boldsymbol{\eta}^p) = \sup_{\boldsymbol{\tau},\, \mathbf{t}} \left[\boldsymbol{\tau} \cdot \boldsymbol{\varepsilon}^p + \mathbf{t} \cdot \boldsymbol{\eta}^p - (V_L - V_0)^*(\mathbf{x}, \boldsymbol{\tau}, \mathbf{t})\right], \tag{28}$$

$$\phi_L(\mathbf{x}, \boldsymbol{\varepsilon}^p) = \sup_{\boldsymbol{\rho}} \left[\boldsymbol{\rho} \cdot \boldsymbol{\varepsilon}^p - (\phi_L)^*(\mathbf{x}, \boldsymbol{\rho})\right]. \tag{29}$$

The effective potential $\widetilde{V}_L$ of the LCC is given in terms of the local potentials $V_L$ and $\phi_L$ by an expression analogous to (11). Making use of the identities (28)-(29), the expression becomes

$$\widetilde{V}_L(\overline{\boldsymbol{\varepsilon}}^p) = \sup_{\boldsymbol{\tau}(\mathbf{x}),\, \mathbf{t}(\mathbf{x}),\, \boldsymbol{\rho}(\mathbf{x})} \left\{ \widetilde{V}_0(\overline{\boldsymbol{\varepsilon}}^p) - \frac{1}{\Omega_\#}\left[\int_{\Omega_\#} (V_L - V_0)^*(\mathbf{x}, \boldsymbol{\tau}, \mathbf{t})\, d\Omega + \int_{\Gamma_\#} (\phi_L)^*(\mathbf{x}, \boldsymbol{\rho})\, d\Gamma\right]\right\}, \tag{30}$$

where

$$\widetilde{V}_0(\overline{\boldsymbol{\varepsilon}}^p) = \inf_{(\boldsymbol{\varepsilon}', \boldsymbol{\varepsilon}^{p'}) \in \mathcal{K}_\#} \frac{1}{\Omega_\#}\left\{\int_{\Omega_\#} \left[\frac{1}{2}\left(\boldsymbol{\varepsilon}' - \boldsymbol{\varepsilon}^{p'}\right) \cdot \mathbf{L}\left(\boldsymbol{\varepsilon}' - \boldsymbol{\varepsilon}^{p'}\right)\right.\right.$$
$$\left.\left. + V_0(\overline{\boldsymbol{\varepsilon}}^p + \boldsymbol{\varepsilon}^{p'}, \nabla\boldsymbol{\varepsilon}^{p'}) + \boldsymbol{\tau} \cdot (\overline{\boldsymbol{\varepsilon}}^p + \boldsymbol{\varepsilon}^{p'}) + \mathbf{t} \cdot \nabla\boldsymbol{\varepsilon}^{p'}\right] d\Omega + \int_{\Gamma_\#} \boldsymbol{\rho} \cdot (\overline{\boldsymbol{\varepsilon}}^p + \boldsymbol{\varepsilon}^{p'})\, d\Gamma\right\}. \tag{31}$$

Following Fleck and Willis [10] and Aifantis and Willis [14], a lower bound for $\widetilde{V}_L$ is now generated by restricting the polarization fields in (30) to[1]

$$\boldsymbol{\tau}(\mathbf{x}) = \sum_{r=1}^{N} \chi_\Omega^{(r)}(\mathbf{x})\boldsymbol{\tau}^{(r)}, \quad \mathbf{t}(\mathbf{x}) = \mathbf{0}, \quad \boldsymbol{\rho}(\mathbf{x}) = \sum_{i=1}^{M} \chi_\Gamma^{(i)}(\mathbf{x})\boldsymbol{\rho}^{(i)}. \tag{32}$$

Recall that the infimum for $\widetilde{V}_0$ in (31) is obtained by setting the first variation with respect to $\boldsymbol{\varepsilon}'$ and $\boldsymbol{\varepsilon}^{p'}$ equal to zero. At the infimum, the equilibrium equations hold,

$$L_{ijkl}\left(u'_{k,lj} - \varepsilon^{p'}_{kl,j}\right) = 0, \tag{33}$$

[1]Sharper bounds could obviously be obtained by using a field $\mathbf{t}(\mathbf{x})$ which is uniform within each phase, but at the expense of more complicated computations.

$$(M^{(0)}+L)_{ijkl}\varepsilon^{p'}_{kl} - N^{(0)}_{ijklmn}\varepsilon^{p'}_{lm,nk} - L_{ijkl}u'_{k,l} + \tau'_{ij} + \int_{\Gamma_\#}\left(\delta(\mathbf{x}-\mathbf{y}) - \Omega^{-1}_\#\right)\rho_{ij}(\mathbf{y})d\Gamma(\mathbf{y}) = 0, \quad (34)$$

where $\boldsymbol{\varepsilon}' = \mathrm{sym}(\nabla\mathbf{u}')$ and $\boldsymbol{\tau}' = \boldsymbol{\tau} - \overline{\boldsymbol{\tau}}$. This linear system of partial differential equations can be solved using Fourier analysis as shown in Appendix A. In particular, the plastic strain fluctuation is given by

$$\boldsymbol{\varepsilon}^{p'}(\mathbf{x}) = -\sum_{\boldsymbol{\xi}\,\in\,\mathcal{R}_0^*}\hat{\boldsymbol{\Lambda}}(\boldsymbol{\xi})\left[\sum_{r=1}^{N}c^{(r)}G^{(r)}_\Omega(-\boldsymbol{\xi})\boldsymbol{\tau}^{(r)} + \sum_{i=1}^{M}p^{(i)}G^{(i)}_\Gamma(-\boldsymbol{\xi})\boldsymbol{\rho}^{(i)}\right]e^{\mathrm{i}\boldsymbol{\xi}\,\cdot\,\mathbf{x}}, \quad (35)$$

where the operator $\hat{\boldsymbol{\Lambda}}(\boldsymbol{\xi})$ and the functions $G^{(r)}_\Omega(\boldsymbol{\xi})$ and $G^{(i)}_\Gamma(\boldsymbol{\xi})$ are given in Appendix A, and $\mathcal{R}_0^*$ denotes the set of reciprocal lattice vectors (in Fourier space) excluding the zero vector.

Now introduce the notation $\langle\cdot\rangle^{(r)}_\Omega$ for the volume average over phase $r$, and similarly, $\langle\cdot\rangle^{(i)}_\Gamma$ for the surface average over $\Gamma^{(i)}$. Making use of the equilibrium equations (33)-(34), the effective potential $\widetilde{V}_0$ can be written in terms of $\boldsymbol{\varepsilon}^{p'}$ only:

$$\widetilde{V}_0(\overline{\boldsymbol{\varepsilon}}^p) = \frac{1}{2}\overline{\boldsymbol{\varepsilon}}^p\cdot\mathbf{M}^{(0)}\overline{\boldsymbol{\varepsilon}}^p + \sum_{r=1}^{N}c^{(r)}\boldsymbol{\tau}^{(r)}\cdot\left(\overline{\boldsymbol{\varepsilon}}^p + \frac{1}{2}\langle\boldsymbol{\varepsilon}^{p'}\rangle^{(r)}_\Omega\right) + \sum_{i=1}^{M}p^{(i)}\boldsymbol{\rho}^{(i)}\cdot\left(\overline{\boldsymbol{\varepsilon}}^p + \frac{1}{2}\langle\boldsymbol{\varepsilon}^{p'}\rangle^{(i)}_\Gamma\right). \quad (36)$$

This expression only requires the average of the plastic strain field (35) over each phase and interface. These are given by

$$\langle\boldsymbol{\varepsilon}^{p'}\rangle^{(r)}_\Omega = -\sum_{s=1}^{N}c^{(s)}\mathbf{P}^{(rs)}\boldsymbol{\tau}^{(s)} - \sum_{j=1}^{M}p^{(j)}\mathbf{Q}^{(rj)}\boldsymbol{\rho}^{(j)}, \quad (37)$$

$$\langle\boldsymbol{\varepsilon}^{p'}\rangle^{(i)}_\Gamma = -\sum_{s=1}^{N}c^{(s)}\mathbf{Q}^{(is)}\boldsymbol{\tau}^{(s)} - \sum_{j=1}^{M}p^{(j)}\mathbf{R}^{(ij)}\boldsymbol{\rho}^{(j)}, \quad (38)$$

where the microstructural tensors $\mathbf{P}^{(rs)}$, $\mathbf{Q}^{(js)}$ and $\mathbf{R}^{(ij)}$ are defined as

$$\mathbf{P}^{(rs)} = \sum_{\boldsymbol{\xi}\,\in\,\mathcal{R}_0^*}\hat{\boldsymbol{\Lambda}}(\boldsymbol{\xi})G^{(r)}_\Omega(-\boldsymbol{\xi})G^{(s)}_\Omega(\boldsymbol{\xi}), \quad (39)$$

$$\mathbf{Q}^{(js)} = \sum_{\boldsymbol{\xi}\,\in\,\mathcal{R}_0^*}\hat{\boldsymbol{\Lambda}}(\boldsymbol{\xi})G^{(j)}_\Gamma(-\boldsymbol{\xi})G^{(s)}_\Omega(\boldsymbol{\xi}), \quad (40)$$

$$\mathbf{R}^{(ij)} = \sum_{\boldsymbol{\xi}\,\in\,\mathcal{R}_0^*}\hat{\boldsymbol{\Lambda}}(\boldsymbol{\xi})G^{(i)}_\Gamma(-\boldsymbol{\xi})G^{(j)}_\Gamma(\boldsymbol{\xi}). \quad (41)$$

Note from (A9) that the operator $\hat{\boldsymbol{\Lambda}}(\boldsymbol{\xi})$ is such that $\hat{\boldsymbol{\Lambda}}(\boldsymbol{\xi}) = \hat{\boldsymbol{\Lambda}}(-\boldsymbol{\xi})$, and therefore the tensors $\mathbf{P}^{(rs)}$, $\mathbf{Q}^{(is)}$ and $\mathbf{R}^{(ij)}$ are symmetric in their superscripts.

In turn, the Legendre-Fenchel transforms (26)-(27) can be obtained explicitly. For each phase and interface, they are given by

$$(V^{(r)}_L - V_0)^*(\boldsymbol{\tau}^{(r)}, \mathbf{0}) = \frac{1}{2}\boldsymbol{\tau}^{(r)}\cdot\left(\mathbf{M}^{(r)} - \mathbf{M}^{(0)}\right)^{-1}\boldsymbol{\tau}^{(r)}, \quad (42)$$

$$\phi^*_L(\boldsymbol{\rho}^{(i)}) = \frac{1}{2}\boldsymbol{\rho}^{(i)}\cdot(\mathbf{S}^{(i)})^{-1}\boldsymbol{\rho}^{(i)}. \quad (43)$$

Expression (42) has been evaluated at $\mathbf{t} = \mathbf{0}$ in view of the trial field (32).

Introducing (36)-(38) and (42)-(43) into (30), we obtain

$$\widetilde{V}_L(\overline{\boldsymbol{\varepsilon}}^p) \geq \sup_{\boldsymbol{\tau}^{(r)},\boldsymbol{\rho}^{(i)}} \left\{ \frac{1}{2}\overline{\boldsymbol{\varepsilon}}^p \cdot \mathbf{M}^{(0)}\overline{\boldsymbol{\varepsilon}}^p + \left( \sum_{r=1}^{N} c^{(r)}\boldsymbol{\tau}^{(r)} + \sum_{i=1}^{M} p^{(i)}\boldsymbol{\rho}^{(i)} \right) \cdot \overline{\boldsymbol{\varepsilon}}^p \right.$$
$$-\frac{1}{2}\sum_{r=1}^{N}\sum_{s=1}^{N} c^{(r)}c^{(s)}\boldsymbol{\tau}^{(r)} \cdot \mathbf{P}^{(rs)}\boldsymbol{\tau}^{(s)} - \sum_{r=1}^{N}\sum_{i=1}^{M} c^{(r)}p^{(i)}\boldsymbol{\tau}^{(r)} \cdot \mathbf{Q}^{(ri)}\boldsymbol{\rho}^{(i)}$$
$$-\frac{1}{2}\sum_{i=1}^{M}\sum_{j=1}^{M} p^{(i)}p^{(j)}\boldsymbol{\rho}^{(i)} \cdot \mathbf{R}^{(ij)}\boldsymbol{\rho}^{(j)} - \frac{1}{2}\sum_{r=1}^{N} c^{(r)}\boldsymbol{\tau}^{(r)} \cdot \left(\mathbf{M}^{(r)} - \mathbf{M}^{(0)}\right)^{-1}\boldsymbol{\tau}^{(r)}$$
$$\left. -\frac{1}{2}\sum_{i=1}^{M} p^{(i)}\boldsymbol{\rho}^{(i)} \cdot (\mathbf{S}^{(i)})^{-1}\boldsymbol{\rho}^{(i)} \right\}. \tag{44}$$

The optimal polarizations satisfy the stationarity conditions

$$\left(\mathbf{M}^{(r)} - \mathbf{M}^{(0)}\right)^{-1}\boldsymbol{\tau}^{(r)} + \sum_{s=1}^{N} c^{(s)}\mathbf{P}^{(rs)}\boldsymbol{\tau}^{(s)} + \sum_{j=1}^{M} p^{(j)}\mathbf{Q}^{(rj)}\boldsymbol{\rho}^{(j)} = \overline{\boldsymbol{\varepsilon}}^p, \tag{45}$$

$$(\mathbf{S}^{(i)})^{-1}\boldsymbol{\rho}^{(i)} + \sum_{s=1}^{N} c^{(s)}\mathbf{Q}^{(is)}\boldsymbol{\tau}^{(s)} + \sum_{j=1}^{M} p^{(j)}\mathbf{R}^{(ij)}\boldsymbol{\rho}^{(j)} = \overline{\boldsymbol{\varepsilon}}^p. \tag{46}$$

Making use of these relations, expression (44) can be simplified to

$$\widetilde{V}_L(\overline{\boldsymbol{\varepsilon}}^p) \geq \frac{1}{2}\overline{\boldsymbol{\varepsilon}}^p \cdot \mathbf{M}^{(0)}\overline{\boldsymbol{\varepsilon}}^p + \frac{1}{2}\left( \sum_{r=1}^{N} c^{(r)}\boldsymbol{\tau}^{(r)} + \sum_{i=1}^{M} p^{(i)}\boldsymbol{\rho}^{(i)} \right) \cdot \overline{\boldsymbol{\varepsilon}}^p, \tag{47}$$

where $\boldsymbol{\tau}^{(r)}$ and $\boldsymbol{\rho}^{(i)}$ denote the optimal polarizations. Since (45)-(46) are linear relations, the optimal polarizations can be expressed in the form $\boldsymbol{\tau}^{(r)} = \mathbf{B}_{\Omega}^{(r)}\overline{\boldsymbol{\varepsilon}}^p$ and $\boldsymbol{\rho}^{(i)} = \mathbf{B}_{\Gamma}^{(i)}\overline{\boldsymbol{\varepsilon}}^p$, so that, finally,

$$\widetilde{V}_L(\overline{\boldsymbol{\varepsilon}}^p) \geq \frac{1}{2}\overline{\boldsymbol{\varepsilon}}^p \cdot \widetilde{\mathbf{M}}\overline{\boldsymbol{\varepsilon}}^p, \quad \text{with} \quad \widetilde{\mathbf{M}} = \mathbf{M}^{(0)} + \sum_{r=1}^{N} c^{(r)}\mathbf{B}_{\Omega}^{(r)} + \sum_{i=1}^{M} p^{(i)}\mathbf{B}_{\Gamma}^{(i)}. \tag{48}$$

This is the Hashin-Shtrikman lower bound for the effective potential $\widetilde{V}_L$.

In addition, following arguments given in [24], it can be shown that estimates for the corresponding phase and interface averages of the plastic strain are given by expressions (37)-(38) evaluated at the optimal polarizations.

**3.3.2** ***Hashin-Shtrikman and self-consistent estimates.*** In the context of linear composites with gradient effects but without interfaces (*i.e.*, $\phi \equiv 0$), Smyshlyaev and Fleck [26, 27] and Fleck and Willis [10] derived Hashin-Shtrikman *upper* bounds by choosing a homogeneous reference solid (25) with $\mathbf{M}^{(0)}$ and $\mathbf{N}^{(0)}$ in such a way that the function $(V_L - V_0)(\mathbf{x}, \boldsymbol{\varepsilon}^p, \boldsymbol{\eta}^p)$ is concave in $\boldsymbol{\varepsilon}^p$ and $\boldsymbol{\eta}^p$, rather than convex. In that case, use of the concave polar leads to an infimum in (26) rather than a supremum. Consequently, the sense of the inequality in (48) is inverted and an upper bound is achieved. No such upper bound exists, however, when interfaces are added. The root cause is that relation (27) remains preserved with a supremum in place. Relation (30) then involves an infimum over $\boldsymbol{\tau}$ and $\mathbf{t}$ but a supremum over $\boldsymbol{\rho}$, and therefore upper bounds cannot be generated following the above strategy.

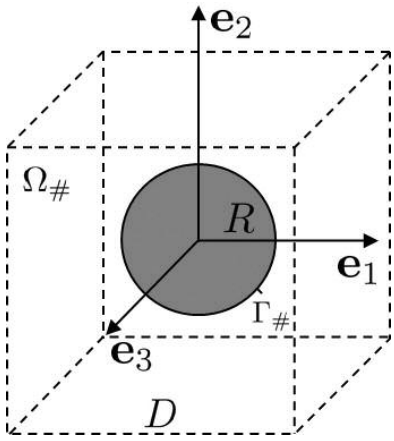


Figure 2. Unit cell.

However, a stationary principle can be stated wherein (26)-(30) involve stationary operations rather than extrema. The inequality (48) is then replaced by an approximation. The specific choice of reference solid now depends on the morphology of the composite under consideration. Estimates of these type have previously been developed for conventional linear composites (*e.g.*, [25, 28]). It is found that the estimates generally give accurate predictions for 'particulate' composites provided the reference solid is identified with the matrix. In applications to follow we shall consider a particulate composite. Thus, we set the tensors $\mathbf{M}^{(0)}$ and $\mathbf{N}^{(0)}$ to equal those of the matrix phase. Denote the matrix phase by $r = 1$. Then, expression $(48)_2$ for $\widetilde{\mathbf{M}}$ takes the form

$$\widetilde{\mathbf{M}} = \mathbf{M}^{(1)} + \sum_{r=2}^{N} c^{(r)} \mathbf{B}_\Omega^{(r)} + \sum_{i=1}^{M} p^{(i)} \mathbf{B}_\Gamma^{(i)}. \tag{49}$$

Evidently, if the matrix material is the more compliant phase in the composite, then this estimate constitutes a lower bound.

A self-consistent estimate for the effective properties of a general composite with interfaces is now derived. In the context of conventional linear composites, it is well-known that a self-consistent estimate for the relevant effective tensor results from identifying the reference tensor in the Hashin-Shtrikman procedure with the effective tensor itself [25]. The resulting estimate treats every phase in a symmetric fashion, and is therefore consistent with the character of a 'granular' microstructure[1]. Now, consider linear composites with gradient effects. The tensors $\mathbf{B}_\Omega^{(r)}$ and $\mathbf{B}_\Gamma^{(i)}$ in $(48)_2$ each depend upon $\mathbf{M}^{(0)}$ and $\mathbf{N}^{(0)}$. Thus, a self-consistent estimate can be obtained by equating $\mathbf{M}^{(0)}$ to $\widetilde{\mathbf{M}}$ and by relating $\mathbf{N}^{(0)}$ to $\widetilde{\mathbf{M}}$ by some suitable prescription which will depend on the specific problem considered. For instance, Fleck and Willis [10] derived self-consistent estimates for two-phase isotropic composites by letting $\mathbf{N}^{(0)} = 3\ell^2(\mathbf{K} \cdot \widetilde{\mathbf{M}})\mathcal{L}$ (see below for definition of symbols). Relation $(48)_2$ then becomes an implicit equation for $\widetilde{\mathbf{M}}$. In the current study, the emphasis is placed on particulate composites rather than granular composites, and the self-consistent approach is not developed further.

## 4 Application to particle-reinforced power-law composites

For illustrative purposes, the nonlinear estimates derived in the previous section are specialized here to power-law materials reinforced by a periodic array of spherical inclusions of radius $R$. The inclusions are assumed to be located at the centers of cubic unit cells of side $D$, as shown in fig. 2. The resulting

[1]In granular composites, all phases play the role of 'grains', as in a polycrystal, and there is no clearly defined matrix phase.

estimates should be relevant, for instance, for modeling the influence of inclusion size observed in metal-matrix composites with reinforcement sizes in the range of $0.1-10\mu$m [1,2]. Such inclusions are sufficiently small for geometrically necessary dislocations to contribute significantly to the material hardening, while sufficiently large to interact with a large number of dislocations. The numerical examples below, however, are not intended to represent any particular set of experiments.

The matrix and inclusion phases will be denoted by $r=1$ and $r=2$, respectively. Thus, the volume fractions of the phases and the surface area-to-volume ratio of the interface are, respectively,

$$c^{(2)}=1-c^{(1)}=\frac{4}{3}\pi\left(\frac{R}{D}\right)^3 \quad \text{and} \quad p\equiv p^{(1)}=4\pi\frac{R^2}{D^3}=\frac{3}{R}c^{(2)}. \tag{50}$$

Both phases are assumed to be isotropic, incompressible solids. Recall that in the present study the elastic modulus $\mathbf{L}$ is spatially uniform, and it can be written as $\mathbf{L}=2\mu\mathbf{K}$, where $\mu$ is the shear modulus and $\mathbf{K}$ is the standard fourth-order, isotropic shear projection tensor. Following Fleck and Willis [10], the plastic potentials (15) are taken to be power-law functions of the form

$$V^{(r)}(\boldsymbol{\varepsilon}^p,\boldsymbol{\eta}^p)=\frac{\sigma_0^{(r)}\varepsilon_0}{1+m}\left(\frac{E_p}{\varepsilon_0}\right)^{1+m}, \quad \text{with} \quad E_p^2=\frac{2}{3}\left[\boldsymbol{\varepsilon}^p\cdot\boldsymbol{\varepsilon}^p+\ell^2\boldsymbol{\eta}^p\cdot\boldsymbol{\eta}^p\right]=\varepsilon_p^2+\frac{2}{3}\ell^2\boldsymbol{\eta}^p\cdot\boldsymbol{\eta}^p, \tag{51}$$

where $\sigma_0^{(r)}$ is the flow stress of phase $r$, $m$ is the hardening index, such that $0\le m\le 1$, $\varepsilon_0$ is a reference strain, and $\ell$ is a material parameter representing the plasticity length scale. For simplicity, $m$, $\ell$, and $\varepsilon_0$ are taken to be the same for both phases. When $\ell=0$, $E_p$ reduces to the standard von Mises plastic strain measure $\varepsilon_p=\sqrt{(2/3)\boldsymbol{\varepsilon}^p\cdot\boldsymbol{\varepsilon}^p}$.

In turn, the interface $\Gamma\equiv\Gamma^{(1)}$ between the two phases is characterized by a power-law potential

$$\phi(\boldsymbol{\varepsilon}^p)\equiv\phi^{(1)}(\boldsymbol{\varepsilon}^p)=\frac{\tau_0\varepsilon_0}{1+n}\left(\frac{\varepsilon_p}{\varepsilon_0}\right)^{1+n}, \quad \text{with} \quad \tau_0=\kappa\ell(\sigma_0^{(1)}\sigma_0^{(2)})^{1/2}. \tag{52}$$

In this expression, the exponent $n$ is such that $0\le n\le 1$, $\varepsilon_0$ is the same as in (51), for simplicity, and $\tau_0$ is a parameter representing the resistance of the interface to plastic slip, characterized by the non-dimensional parameter $\kappa$. The form $(52)_2$ for $\tau_0$ is an arbitrary choice with the required dimensions of stress×length (*cf.* (5) ). The limiting values of the exponent $n=1$ and $n=0$ correspond to linear and 'rigid-perfectly plastic' interfaces, respectively. Linear interfaces have been used by Borg and Fleck [21], for instance, to model surface roughening in bicrystals, while 'rigid-perfectly plastic' interfaces have been used by Aifantis and Willis [12,14] to model dislocation pile-ups in polycrystalline materials.

### 4.1 *Elementary bounds*

The Voigt upper bound for the composite (50)-(52) follows directly from (16), to give

$$\widetilde{V}(\overline{\boldsymbol{\varepsilon}}^p)\le\frac{\sigma_V\varepsilon_0}{1+m}\left(\frac{\overline{\varepsilon}_p}{\varepsilon_0}\right)^{1+m}+p\,\frac{\tau_0\varepsilon_0}{1+n}\left(\frac{\overline{\varepsilon}_p}{\varepsilon_0}\right)^{1+n}, \quad \sigma_V=c^{(1)}\sigma_0^{(1)}+c^{(2)}\sigma_0^{(2)}, \tag{53}$$

where $\sigma_V$ is the classical Voigt bound on the effective flow stress of a power-law composite.

In turn, the Reuss bound is obtained by introducing (51) into (17), giving

$$\widetilde{V}(\overline{\boldsymbol{\varepsilon}}^p)\ge\frac{\sigma_R\varepsilon_0}{1+m}\left(\frac{\overline{\varepsilon}_p}{\varepsilon_0}\right)^{1+m}, \quad \sigma_R=\left(\frac{c^{(1)}}{(\sigma_0^{(1)})^{1/m}}+\frac{c^{(2)}}{(\sigma_0^{(2)})^{1/m}}\right)^{-m}, \tag{54}$$

where $\sigma_R$ is the classical Reuss bound on the effective flow stress of a power-law composite.

### 4.2 *Nonlinear estimates of Hashin-Shtrikman type*

In view of the 'particulate' character of the microstructure considered, refined estimates are obtained here by making use of the nonlinear variational estimate (20) in conjuction with the linear Hashin-Shtrikman estimate (49).

Motivated by the particular form of the potentials (51) and (52), we restrict the potentials (18) and (19) in the LCC to the form

$$V_L^{(r)}(\boldsymbol{\varepsilon}^p, \boldsymbol{\eta}^p) = \frac{1}{2} b^{(r)} E_p^2, \quad \phi_L(\boldsymbol{\varepsilon}^p) = \frac{1}{2}\alpha \varepsilon_p^2, \tag{55}$$

where $b^{(r)} \geq 0$ and $\alpha \geq 0$. This amounts to restricting the set of tensors $\mathbf{M}^{(r)}$, $\mathbf{N}^{(r)}$ and $\mathbf{S} \equiv \mathbf{S}^{(1)}$ in (20) to those of the form

$$\mathbf{M}^{(r)} = \frac{2}{3} b^{(r)} \mathbf{K}, \quad \mathbf{N}^{(r)} = \frac{2}{3} b^{(r)} \ell^2 \mathcal{L}, \quad \mathbf{S} = \frac{2}{3}\alpha \mathbf{K}, \tag{56}$$

where $\mathcal{L}$ is the sixth-order incompressible identity tensor with components $\mathcal{L}_{ijklmn} = (\delta_{il}\delta_{jm}\delta_{kn} + \delta_{jl}\delta_{im}\delta_{kn})/2 - \delta_{ij}\delta_{lm}\delta_{kn}/3$.

With this choice of linear comparison potentials, the 'corrector' functions (21) and (22) can be evaluated analytically, and the nonlinear estimate (20) reduces to

$$\widetilde{V}(\overline{\boldsymbol{\varepsilon}}^p) = \inf_{b^{(r)}, \alpha} \left\{ \frac{1}{2}\overline{\boldsymbol{\varepsilon}}^p \cdot \widetilde{\mathbf{M}}\overline{\boldsymbol{\varepsilon}}^p + \sum_{r=1}^{2} c^{(r)} \frac{1-m}{1+m} \frac{\sigma_0^{(r)}\varepsilon_0}{2} \left( \frac{\sigma_0^{(r)}}{\varepsilon_0 b^{(r)}} \right)^{\frac{1+m}{1-m}} + p\frac{1-n}{1+n}\frac{\tau_0\varepsilon_0}{2}\left(\frac{\tau_0}{\varepsilon_0\alpha}\right)^{\frac{1+n}{1-n}} \right\}, \tag{57}$$

where $\widetilde{\mathbf{M}}$ is given in terms of the $b^{(r)}$ and $\alpha$ by (B1), and the minimization procedure is carried out numerically.

### 4.3 *Results and discussion*

The numerical results presented in this section correspond to reinforced materials with hardening index $m = 0.2$, reference strain $\varepsilon_0 = 1$, and reinforcement volume fraction $c^{(2)} = 0.2$, subjected to uniaxial loadings along a reference axis $\mathbf{e}_i$, see fig. 2.

First, in order to explore the effect of interface constitutive behavior on the macroscopic response, the nonlinear Hashin-Shtrikman (HS) estimates (solid lines) and the Voigt upper bound (dotted lines) are compared in fig. 3 for the case of a *uniform* material ($\sigma_0^{(1)} = \sigma_0^{(2)} = \sigma_0 = \mu/100$) with three different types of interfaces, of radius $R = \ell$. Parts a, b and c show the macroscopic uniaxial stress $\overline{\sigma}_e$ versus strain $\overline{\varepsilon}_e$ curve corresponding, respectively, to linear ($n = 1$) interfaces, power-law interfaces with the same exponent as the bulk material ($n = 0.2$), and rigid-perfectly plastic interfaces ($n = 0$), for several values of the strength parameter $\kappa$. The choice $\kappa = 0$ neglects any contribution from the interfaces and corresponds to the bulk uniform response; accordingly, it is labelled 'bulk' in the figures.

It is seen that the HS estimates are sensitive to the interface strength, with the macroscopic yield strength and hardening rate depending upon interface nonlinearity $n$. Linear interfaces have a negligible effect on the yield strength but increase the hardening rate, see fig. 3a. With increasing nonlinearity of the interface, the effective yield strength increases while the hardening rate diminishes, see fig. 3b. In the extreme case of a rigid-perfectly plastic interface, the yield strength increases significantly with increasing interface strength, while the hardening rate is insensitive to interface strength, see fig. 3c. In all cases, the HS estimates satisfy the Voigt upper bound, as they should.

Further insight can be gained by considering the average plastic strain $\overline{\boldsymbol{\varepsilon}}_p^{(r)}$ in each phase domain $r$ and the average value $\overline{\boldsymbol{\varepsilon}}_p^{(\Gamma)}$ at the interfaces. The von Mises measure of the average plastic strains, normalized by the macroscopic plastic strain $\overline{\varepsilon}_p$, are plotted in figs. 3d-f as a function of the macroscopic uniaxial strain $\overline{\varepsilon}_e$. Fig. 3d refers to the linear interface as for fig. 3a, but results are restricted to the choice $\kappa = 4$,

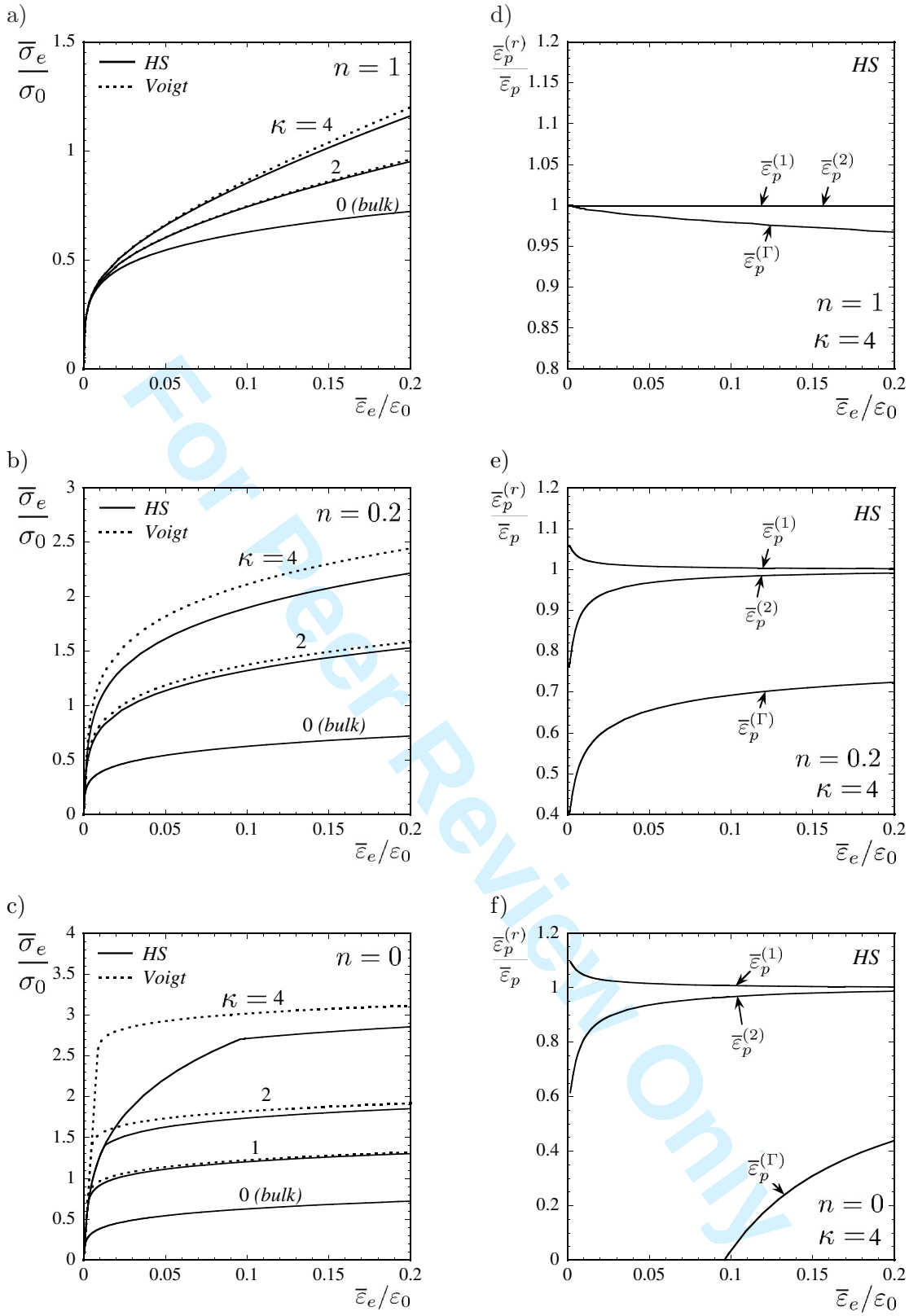


Figure 3. Uniaxial response of a 'uniform' material ($\sigma_0^{(1)} = \sigma_0^{(2)} = \sigma_0$) with interfaces, for $R = \ell$, $c^{(2)} = 0.2$, $m = 0.2$, $\mu/\sigma_0 = 100$, $\varepsilon_0 = 1$. Effect of interface nonlinearity $n$ and strength $\kappa$ on the effective response and the average plastic strain in the matrix ($\overline{\varepsilon}_p^{(1)}$) and inclusion ($\overline{\varepsilon}_p^{(2)}$) domains, and at the interfaces ($\overline{\varepsilon}_p^{(\Gamma)}$). (a) & (d) Linear interfaces ($n = 1$), (b) & (e) nonlinear interfaces with same exponent as bulk material ($n = 0.2$), (c) & (f) rigid-perfectly plastic interfaces ($n = 0$).

where the differences in strain response are greatest. Likewise, figs. 3e and f correspond to the figs. 3b and c, respectively, again with $\kappa = 4$. Linear interfaces tend to deform affinely with the bulk at small strains, and induce plastic heterogeneity only at the larger strains, see fig. 3d. This is consistent with the observation that the macroscopic response in fig. 3a is affected by the presence of interfaces only at the larger strains. As the degree of interface nonlinearity increases, the interface becomes plastically 'stiffer' at low strains, and plastic heterogeneity develops at an earlier stage of deformation, compare figs. 3d and 3e. Consequently, the macroscopic response shows interface strengthening effects at smaller strains. In the extreme case of a rigid-perfectly plastic interface, the HS estimates predict no plastic flow at the interfaces, at low overall strain, see fig. 3f. As the macroscopic deformation proceeds, the plastic strain gradients at the rigid interface increase, until the hyperstress attains the interfacial strength, and the interface yields. At this point, the macroscopic stress versus strain response in fig. 3c exhibits a kink as a result of the sudden drop in the hardening rate. In contrast, the elementary Voigt bound assumes a uniform plastic strain throughout the solid from the initial state: it asserts that the interface yields immediately.

We now turn to particle-reinforced composites ($\sigma_0^{(2)} = 5\sigma_0^{(1)} = 5\mu/100$) containing the three types of interface $n = 0, 0.2$ and 1 as considered above. Hashin-Shtrikman estimates for the macroscopic uniaxial stress versus strain curve are shown in figs. 4a-c, for the choice $\kappa = 1$ and several values of the inclusion radius $R$. The curves labelled $\ell/R = 0$ correspond to a composite with very large inclusions relative to the plasticity length scale. In this limit, the macroscopic response is insensitive to local plastic strain gradients or the presence of interfaces, and conventional particle strengthening is exhibited. When the reinforcement size becomes comparable to the plasticity length scale, the role of plastic strain gradients and interfaces becomes important, giving rise to a significant strengthening effect which can be much larger than that obtained by conventional strengthening alone.

The sensitivity of macroscopic strength to reinforcement size $R$ is explored in figs. 4d-f. Plots are given for the macroscopic uniaxial stress $\overline{\sigma}_e/\sigma_0^{(1)}$ deep in the plastic range at a fixed macroscopic strain $\overline{\varepsilon}_e/\varepsilon_0 = 0.2$, versus the reciprocal of reinforcement size, $\ell/R$. Hashin-Shtrikman estimates for composites with interfacial strengthening ($\kappa = 1$) are compared with HS estimates for similar composites without interfacial strengthening ($\kappa = 0$), and with the elementary bounds. While both sets of HS estimates coincide for large reinforcements ($\ell/R = 0$), as expected, they give divergent predictions with decreasing $R$ and with decreasing $n$. In the absence of interfacial strength ($\kappa = 0$), the HS estimates exhibit a relatively small size effect due to the plastic strain gradients in the bulk. At small $R$, these estimates asymptote to the Voigt bound. As already pointed out in [10], this is a consequence of the fact that strain gradient strengthening forces the plastic strain distribution within the composite to become spatially uniform. In contrast, the presence of interfacial strengthening causes the HS estimates to exhibit a much stronger size effect; they remain well below the corresponding Voigt bound even at small reinforcement sizes. Below a certain size $R$, interface strengthening dominates, and consequently the predicted flow stress scales with the reciprocal of $R$, as dictated by the surface area-to-volume ratio. There exists some experimental evidence for such a scaling in reinforced aluminum-matrix composites with particle diameters and interparticle spacings in the ranges $5 - 50\mu$m and $13 - 100\mu$m [1], for which Orowan strengthening mechanisms are not expected to operate.

In summary, this study has highlighted the sensitivity of macroscopic response to constitutive details of the interface between phases of equal or contrasting strengths. Unravelling the detailed physics of plastic deformation at interfaces remains a challenging fundamental problem.

**Acknowledgements**

This research is based upon work supported by the European Community through the Sixth Framework Programme Integrated Project IP 026467-2 MANUDIRECT, and by the Engineering and Physical Sciences Research Council (EPSRC), UK, through a Materials Modelling Programme.

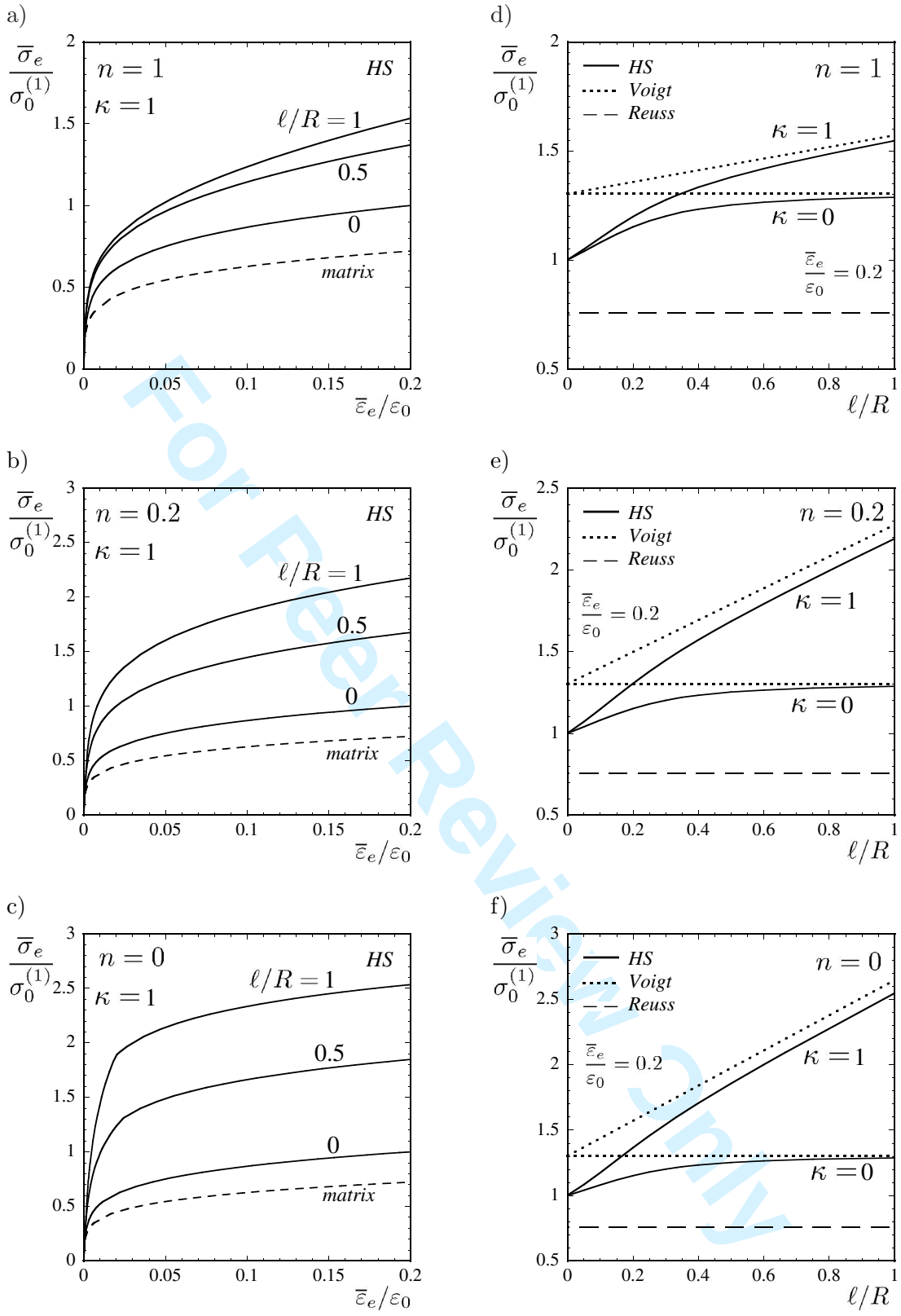


Figure 4. Effect of interface nonlinearity $n$ and particle size $R$ on the uniaxial response of a reinforced composite ($\sigma_0^{(2)}=5\sigma_0^{(1)}=5\mu/100$) with interfaces, with $c^{(2)}=0.2$, $m=0.2$, $\varepsilon_0=1$. (a) & (d) Linear interfaces ($n=1$), (b) & (e) nonlinear interfaces with same exponent as the bulk material ($n=0.2$), (c) & (f) rigid-perfectly plastic interfaces ($n=0$).

## Appendix A: Derivation of the local fields in $\widetilde{V}_0$

The linear system of partial differential equations (33)-(34) can be solved using Fourier analysis. Any periodic function $f(\mathbf{x})$ with period $\Omega_\#$ and zero mean value can be expressed as (*e.g.*, [29,30])

$$f(\mathbf{x}) = \sum_{\boldsymbol{\xi} \in \mathcal{R}_0^*} \hat{f}(\boldsymbol{\xi}) e^{\mathrm{i}\boldsymbol{\xi}\cdot\mathbf{x}}, \quad \hat{f}(\boldsymbol{\xi}) = \frac{1}{\Omega_\#}\int_{\Omega_\#} f(\mathbf{x}) e^{-\mathrm{i}\boldsymbol{\xi}\cdot\mathbf{x}} d\Omega(\mathbf{x}), \tag{A1}$$

where $\mathcal{R}_0^*$ denotes the set of reciprocal lattice vectors excluding the zero vector $\mathbf{0}$.

Making use of this representation for the fields $\mathbf{u}'$ and $\boldsymbol{\varepsilon}^{p'}$ in (33), we have that

$$-L_{ijkl}\left(\xi_l\xi_j\hat{u}'_k + \mathrm{i}\xi_j\hat{\varepsilon}^{p'}_{kl}\right) = 0. \tag{A2}$$

Solving for the Fourier coefficients $\hat{u}'_i$, we obtain

$$\hat{u}'_i = -\mathrm{i}K^{-1}_{im}\xi_j L_{mjkl}\hat{\varepsilon}^{p'}_{kl}, \quad \text{where} \quad K_{ik} = L_{ijkl}\xi_j\xi_l, \tag{A3}$$

and therefore, the Fourier coefficients of the total strain are given by

$$\hat{\varepsilon}'_{ij} = \mathrm{i}\ \hat{u}'_i\xi_j\big|_{(ij)} = \hat{\Gamma}_{ijkl}(\boldsymbol{\xi})L_{klmn}\hat{\varepsilon}^{p'}_{mn}, \quad \text{where} \quad \hat{\Gamma}_{ijkl}(\boldsymbol{\xi}) = K^{-1}_{ik}\xi_j\xi_l\big|_{(ij)(kl)}. \tag{A4}$$

In turn, making use of the represenation (A1) for the fields $\mathbf{u}'$ and $\boldsymbol{\varepsilon}^{p'}$ in (34), and using (A4), we obtain

$$\left[M^{(0)}_{ijkl} + L_{ijkl} + N^{(0)}_{ijmkln}\xi_m\xi_n - L_{ijop}\hat{\Gamma}_{opmn}(\boldsymbol{\xi})L_{mnkl}\right]\hat{\varepsilon}^{p'}_{kl} + \sum_{r=1}^{N} c^{(r)}G^{(r)}_\Omega(-\boldsymbol{\xi})\tau^{(r)}_{ij} + \sum_{i=1}^{M} p^{(i)}G^{(i)}_\Gamma(-\boldsymbol{\xi})\rho^{(i)}_{ij} = 0, \tag{A5}$$

where

$$G^{(r)}_\Omega(\boldsymbol{\xi}) = \frac{1}{\Omega^{(r)}_\#}\int_{\Omega^{(r)}_\#} e^{\mathrm{i}\boldsymbol{\xi}\cdot\mathbf{x}} d\Omega(\mathbf{x}), \tag{A6}$$

$$G^{(i)}_\Gamma(\boldsymbol{\xi}) = \frac{1}{\Gamma^{(i)}_\#}\int_{\Gamma^{(i)}_\#} e^{\mathrm{i}\boldsymbol{\xi}\cdot\mathbf{x}} d\Gamma(\mathbf{x}). \tag{A7}$$

Solving for the Fourier coefficients $\hat{\varepsilon}^{p'}_{ij}$, we obtain

$$\hat{\varepsilon}^{p'}_{ij} = \hat{\Lambda}_{ijkl}(\boldsymbol{\xi})\left[\sum_{r=1}^{N} c^{(r)}\tau^{(r)}_{kl}G^{(r)}_\Omega(-\boldsymbol{\xi}) + \sum_{i=1}^{M} p^{(i)}\rho^{(i)}_{kl}G^{(i)}_\Gamma(-\boldsymbol{\xi})\right], \tag{A8}$$

where the tensor $\hat{\Lambda}$ is defined by

$$\hat{\Lambda}^{-1}_{ijkl}(\boldsymbol{\xi}) = M^{(0)}_{ijkl} + L_{ijkl} + N^{(0)}_{ijmkln}\xi_m\xi_n - L_{ijop}\hat{\Gamma}_{opmn}(\boldsymbol{\xi})L_{mnkl}. \tag{A9}$$

On combining $(\mathrm{A1})_1$ and (A8) we obtain expression (35) for the plastic strain field $\boldsymbol{\varepsilon}^{p'}$.

## Appendix B: Hashin-Shtrikman estimates for a 'particulate' linear composite

The Hashin-Shtrikman estimates (49) are specialized here to composites with a unit cell shown in fig. 2 and local potentials (55). Thus, expression (49) reduces to

$$\widetilde{\mathbf{M}} = \mathbf{M}^{(1)} + c^{(2)}\mathbf{B}_{\Omega}^{(2)} + p\mathbf{B}_{\Gamma}^{(1)}, \tag{B1}$$

where the concentration tensors $\mathbf{B}_{\Omega}^{(2)}$ and $\mathbf{B}_{\Gamma}^{(1)}$ are solution to the system of linear equations

$$\left(\frac{3}{2}\frac{1}{b^{(2)}-b^{(1)}}\mathbf{K} + c^{(2)}\mathbf{P}^{(22)}\right)\mathbf{B}_{\Omega}^{(2)} + p\mathbf{Q}^{(12)}\mathbf{B}_{\Gamma}^{(1)} = \mathbf{K}, \tag{B2}$$

$$c^{(2)}\mathbf{Q}^{(12)}\mathbf{B}_{\Omega}^{(2)} + \left(\frac{3}{2\alpha}\mathbf{K} + p\mathbf{R}^{(11)}\right)\mathbf{B}_{\Gamma}^{(1)} = \mathbf{K}, \tag{B3}$$

arising from the stationarity conditions (45)-(46).

The microstructural tensors $\mathbf{P}^{(22)}$, $\mathbf{R}^{(11)}$ and $\mathbf{Q}^{(12)}$ are given by expressions (39)-(41). In these expressions, the summations must be carried out over the reciprocal lattice $\mathcal{R}_0^*$, which, for the microstructure considered here, is the set of vectors $\boldsymbol{\xi} \neq \mathbf{0}$ of the form (*e.g.*, [29, 30])

$$\boldsymbol{\xi} = \frac{2\pi}{D}\left(n_1\mathbf{e}_1 + n_2\mathbf{e}_2 + n_3\mathbf{e}_3\right), \quad n_i = 0, \pm 1, \pm 2, ... \tag{B4}$$

where the basis vectors $\mathbf{e}_i$ are those shown in fig. 2. In practice, the summations are truncated at sufficiently large values of the components $n_i$, and the symmetries of the unit cell can be used to reduce the range of values. In turn, for modulus tensors of the form (56), the tensor $\hat{\mathbf{\Lambda}}(\boldsymbol{\xi})$ as defined by (A9) reduces to (*cf.* [10])

$$\hat{\mathbf{\Lambda}}(\boldsymbol{\xi}) = \frac{3}{6\mu + 2b^{(1)}(1+\ell^2|\boldsymbol{\xi}|^2)}\mathbf{K} + \frac{9\mu^2}{b^{(1)}(1+\ell^2|\boldsymbol{\xi}|^2)(3\mu + b^{(1)}(1+\ell^2|\boldsymbol{\xi}|^2))}\hat{\mathbf{\Gamma}}(\boldsymbol{\xi}), \tag{B5}$$

where $\hat{\mathbf{\Gamma}}$ has components

$$\hat{\Gamma}_{ijkl}(\boldsymbol{\xi}) = \frac{1}{\mu}\left(\frac{\delta_{ik}\xi_j\xi_l}{|\boldsymbol{\xi}|^2} - \frac{\xi_i\xi_j\xi_k\xi_l}{|\boldsymbol{\xi}|^4}\right)\Bigg|_{(ij)(kl)}. \tag{B6}$$

In deriving (B5), use has been made of the fact that (B6) satisfies the identity $2\mu\hat{\mathbf{\Gamma}}\hat{\mathbf{\Gamma}} = \hat{\mathbf{\Gamma}}$. Finally, the integrals in the definitions (A6)-(A7) of the shape functions $G_{\Omega}^{(2)}$ and $G_{\Gamma}^{(1)}$ can be performed analytically in the case of a spherical inclusion located at the center of the unit cell, giving (*e.g.*, [17, 30])

$$G_{\Omega}^{(2)}(\boldsymbol{\xi}) = \frac{\sin(R\xi) - (R\xi)\cos(R\xi)}{(R\xi)^3}, \quad G_{\Gamma}^{(1)}(\boldsymbol{\xi}) = \frac{\sin(R\xi)}{R\xi}, \tag{B7}$$

where $\xi = |\boldsymbol{\xi}|$.

## References

[1] S. V. Kamat, J. P. Hirth, R. Mehrabian, Acta Metall. **37** 2395 (1989).
[2] C.-W. Nan, D. R. Clarke, Acta Mater. **9** 3801 (1996).
[3] A. Misra, J. P. Hirth, R. G. Hoagland, Acta Mater. **53** 4817 (2005).
[4] L. He, E. Ma, Nanostruct. Mater. **7** 327 (1996).
[5] L. He, L. F. Allard, E. Ma, Scripta Mater. **42** 517 (2000).
[6] P. Ponte Castañeda, P. Suquet, Adv. Appl. Mech. **34** 171 (1998).
[7] J. R. Willis, Eur. J. Mech. A/Solids **19** S165 (2000).

[8] V. P. Smyshlyaev, N. A. Fleck, Proc. R. Soc. Lond. A **451** 795 (1995).
[9] S. H. Chen, T. C. Wang, Acta Mech. **157** 113 (2002).
[10] N. A. Fleck, J. R. Willis, J. Mech. Phys. Solids **52** 1855 (2004).
[11] U. Borg, C. F. Niordson, N. A. Fleck, V. Tvergaard, Int. J. Solids Struct. **43** 4906 (2006).
[12] K. E. Aifantis, J. R. Willis, J. Mech. Phys. Solids **53** 1047 (2005).
[13] M. E. Gurtin, L. Anand, J. Mech. Phys. Solids **56** 184 (2008).
[14] K. E. Aifantis, J. R. Willis, Mech. Materials **38** 702 (2006).
[15] P. Ponte Castañeda, J. Mech. Phys. Solids **39** 45 (1991).
[16] Z. Hashin, S. Shtrikman, J. Mech. Phys. Solids **10** 335 (1962).
[17] S. Nemat-Nasser, T. Iwakuma, M. Hejazi, Mech. Materials **1** 239 (1982).
[18] P. Suquet, C. R. Acad. Sci. Paris II **311** 769 (1990).
[19] N. A. Fleck, J. W. Hutchinson, Adv. Appl. Mech. **33** 295 (1997).
[20] K. E. Aifantis, W. A. Soer, J. Th. M. De Hosson, J. R. Willis, Acta Mater. **54** 5077 (2006).
[21] U. Borg, N. A. Fleck, Modelling Simul. Mater. Sci. Eng. **15** S1 (2007).
[22] M. P. Dewald, W. A. Curtin, Philos. Mag. **87** 4615 (2007).
[23] M. I. Idiart, P. Ponte Castañeda, Proc. R. Soc. A **463** 907 (2007).
[24] M. I. Idiart, P. Ponte Castañeda, Proc. R. Soc. A **463** 183 (2007).
[25] J. R. Willis, J. Mech. Phys. Solids **25** 185 (1977).
[26] V. P. Smyshlyaev, N. A. Fleck, J. Mech. Phys. Solids **42** 1851 (1994).
[27] V. P. Smyshlyaev, N. A. Fleck, J. Mech. Phys. Solids **44** 465 (1996).
[28] P. Ponte Castañeda, J. R. Willis, J. Mech. Phys. Solids **43** 1919 (1995).
[29] C. Kittel, *Introduction to Solid State Physics* (John Wiley & Sons, New York, 1996).
[30] P. Suquet, Internal Report, L.M.A. Marseille (1990).

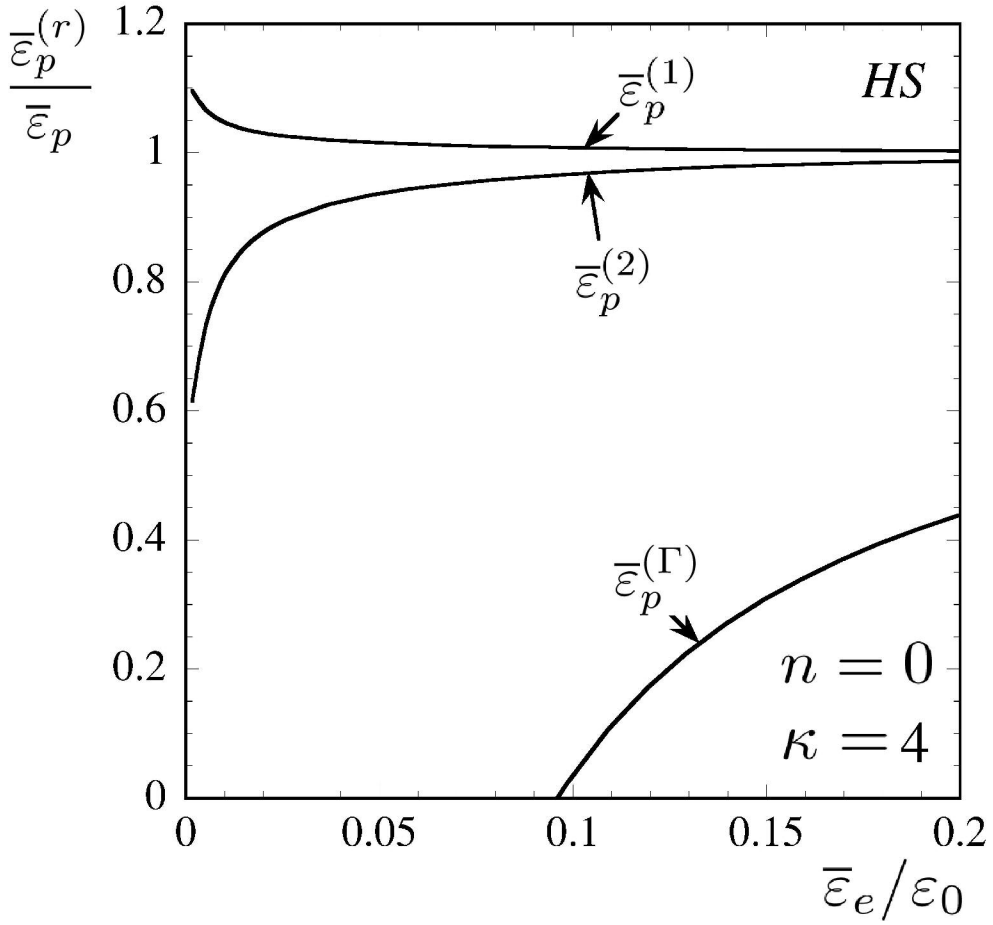


**3f**
164x151mm (600 x 600 DPI)

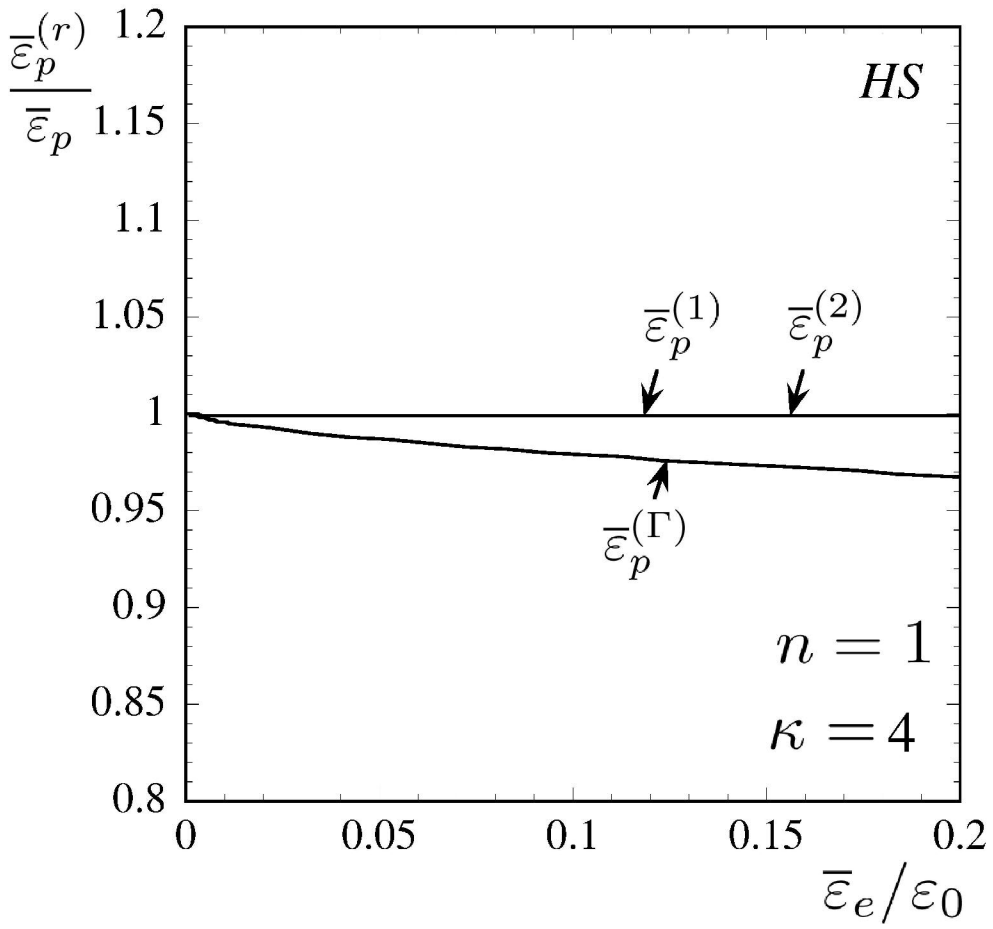


**3d**
164x151mm (600 x 600 DPI)

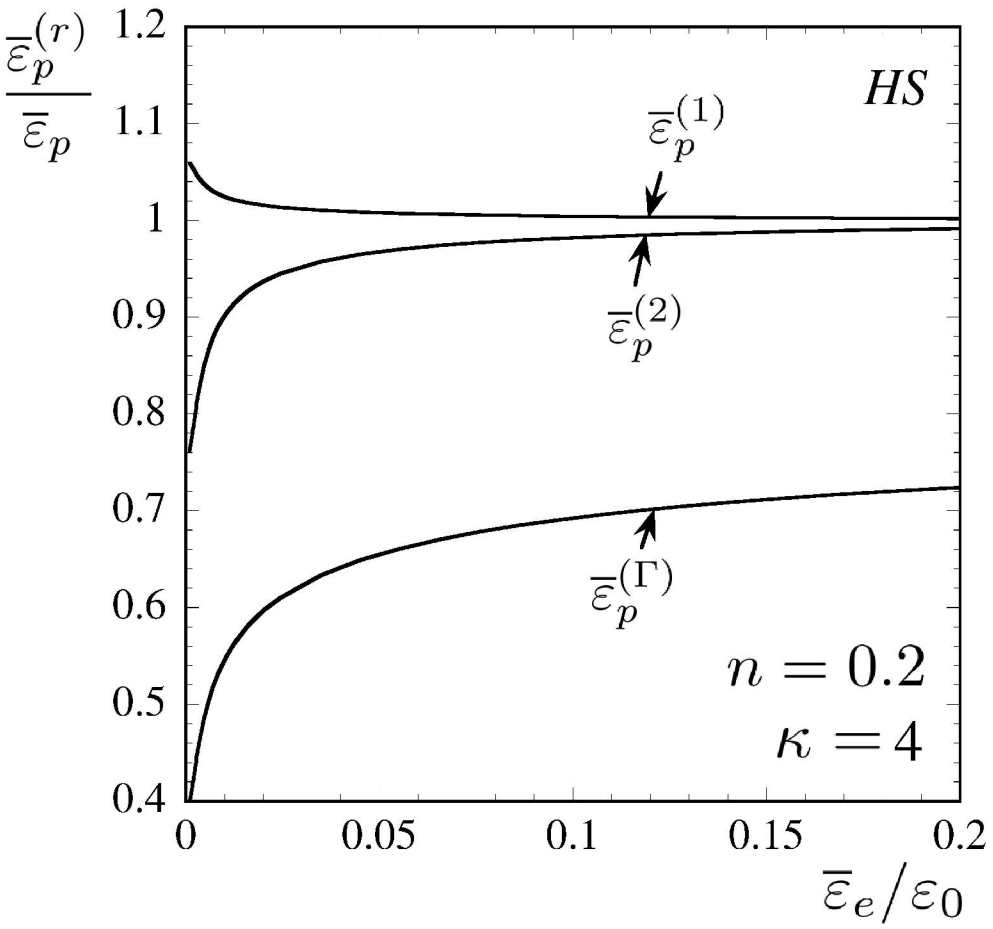


**3e**
164x151mm (600 x 600 DPI)

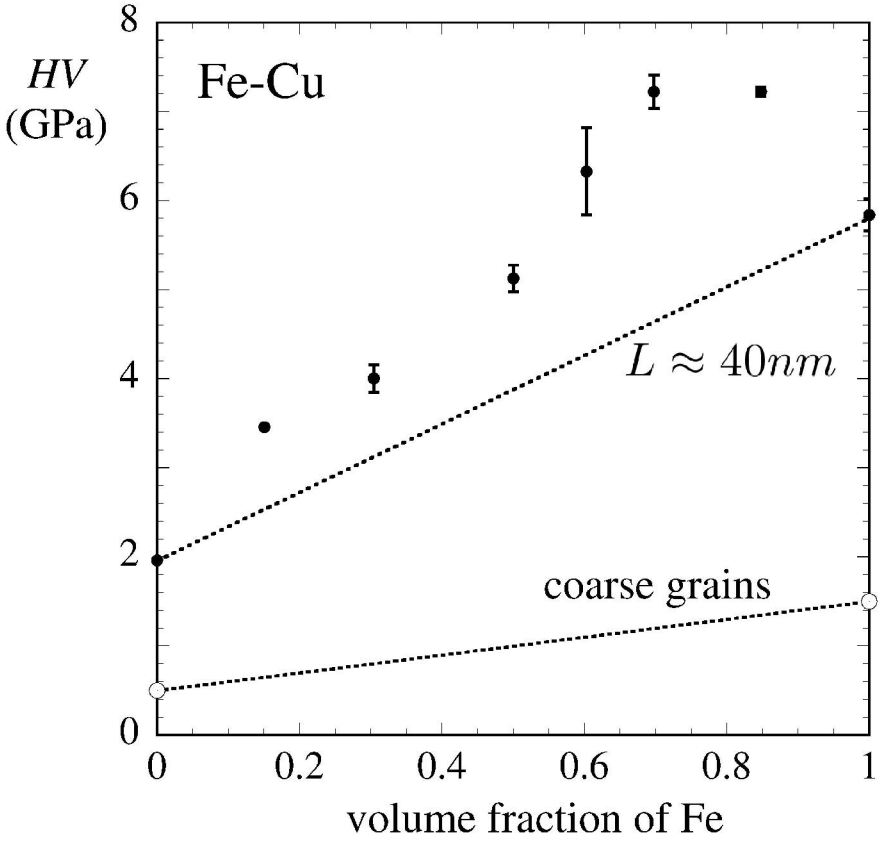


**1a**
178x152mm (600 x 600 DPI)

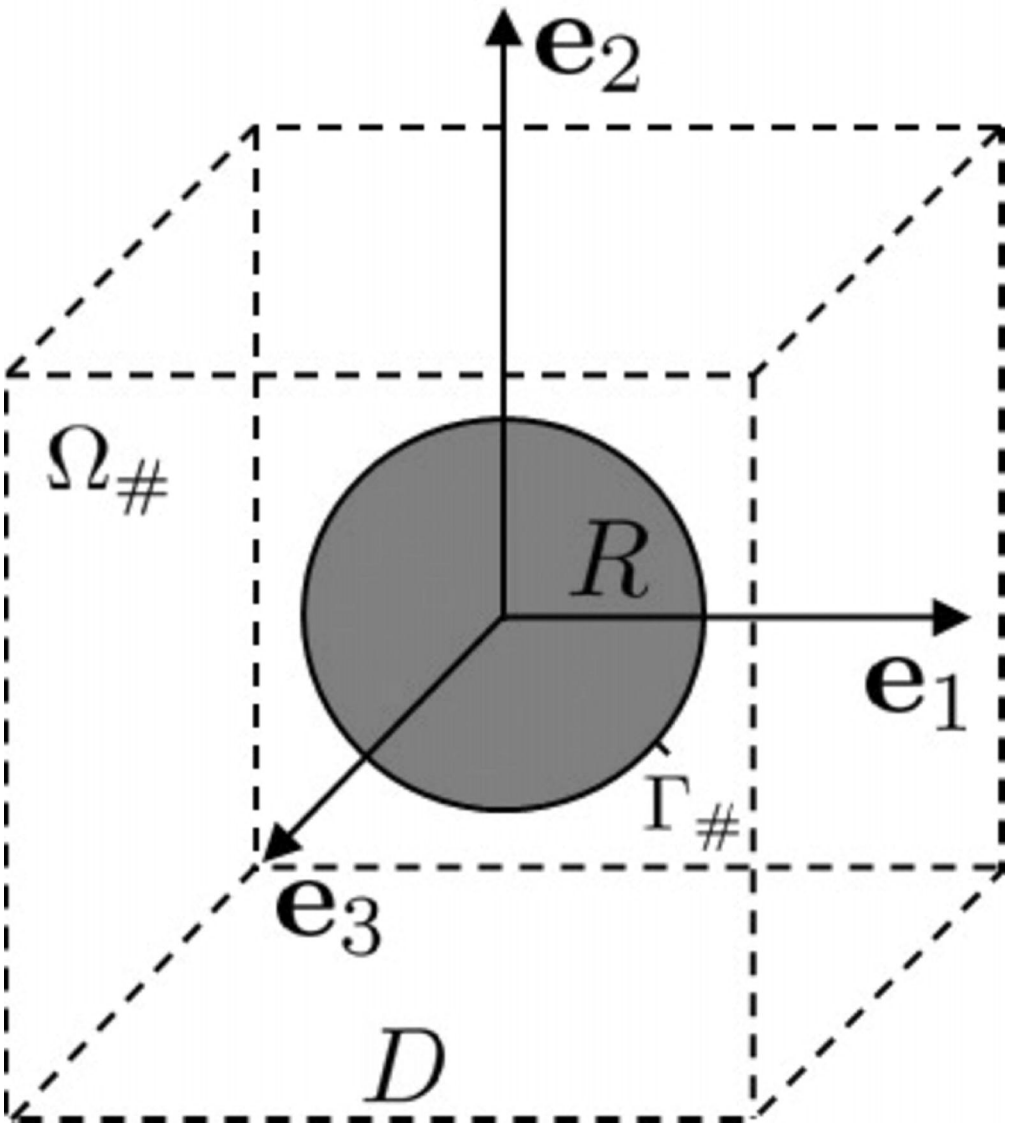


**2**
119x134mm (600 x 600 DPI)

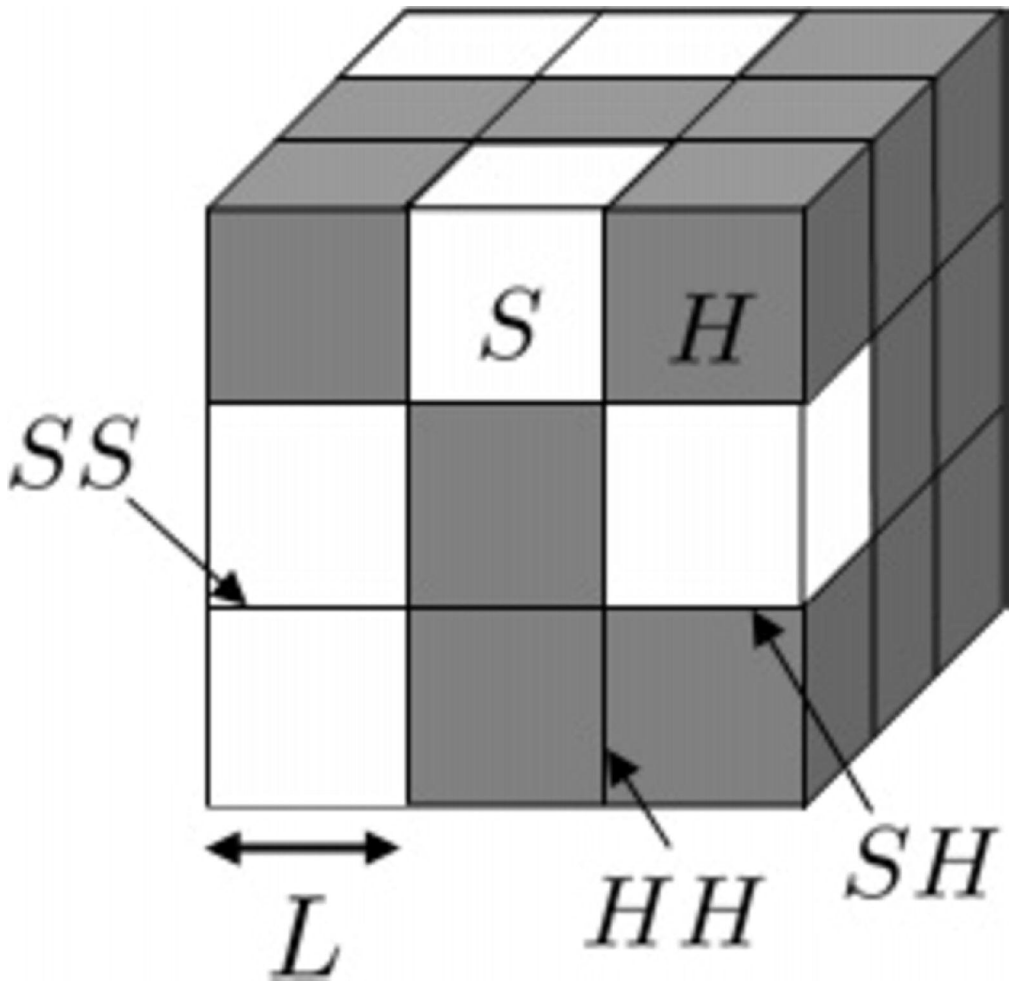


**Table 1 left**
79x77mm (600 x 600 DPI)

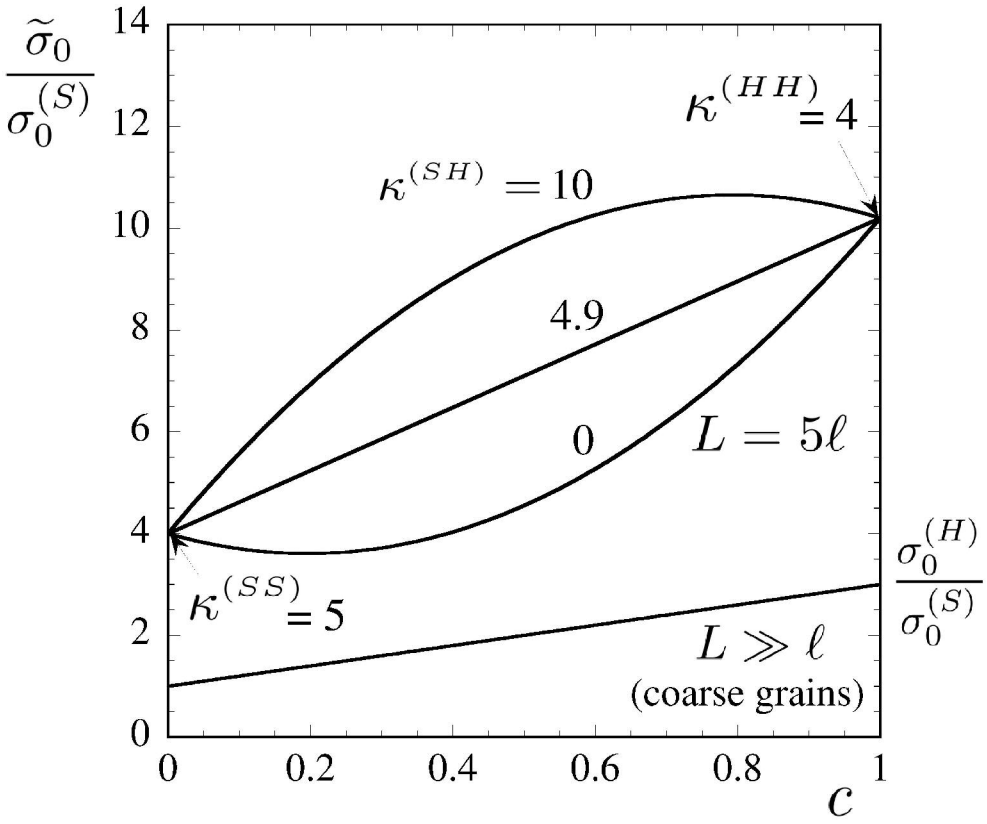


**1b**
178x152mm (600 x 600 DPI)

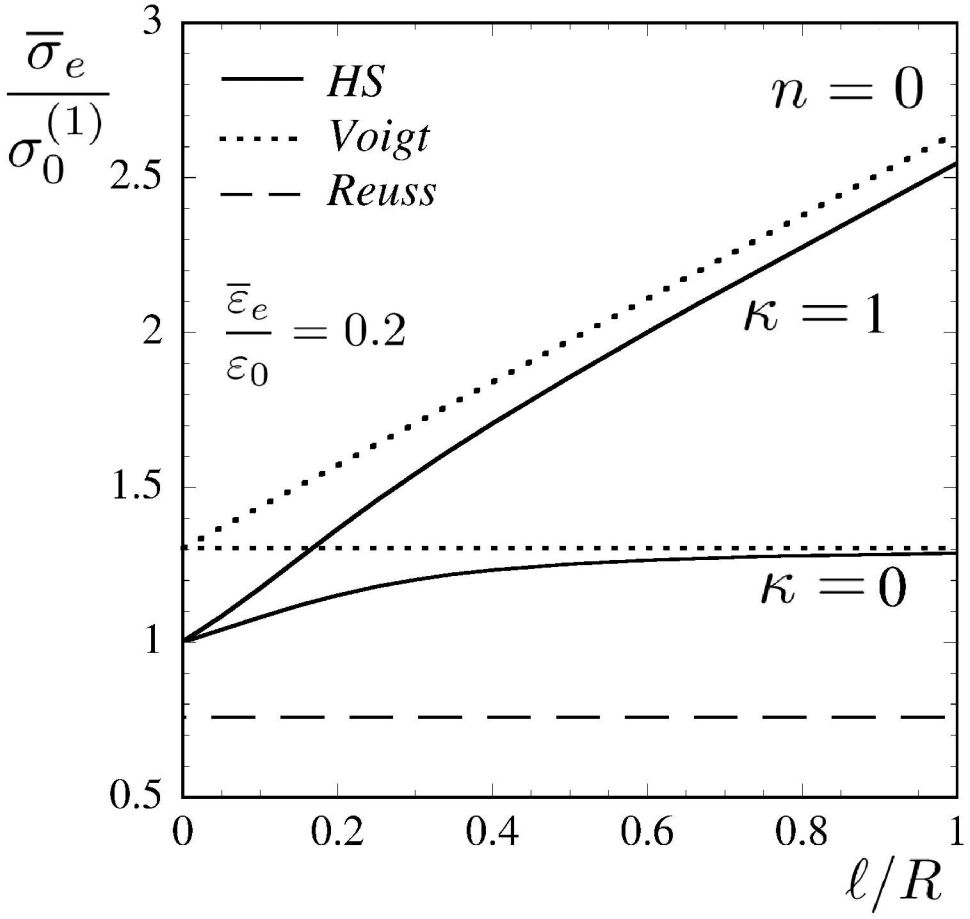


**4f**
164x151mm (600 x 600 DPI)

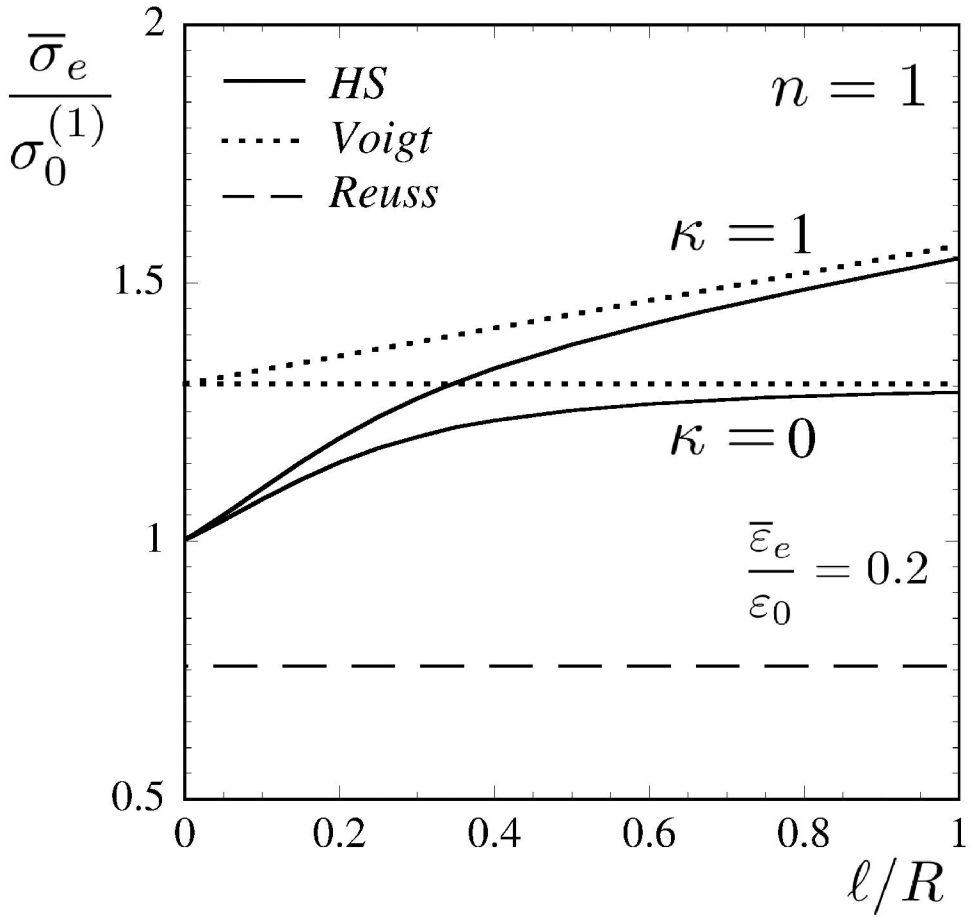


**4d**
164x151mm (600 x 600 DPI)

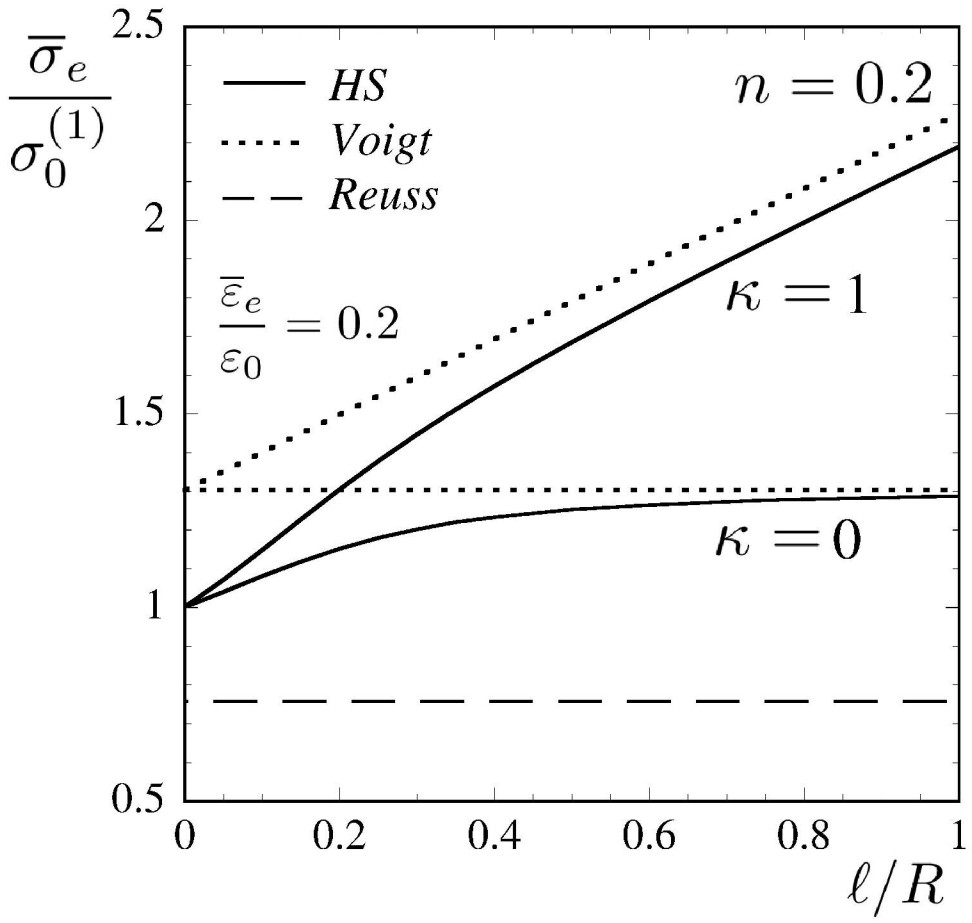


**4e**
164x151mm (600 x 600 DPI)

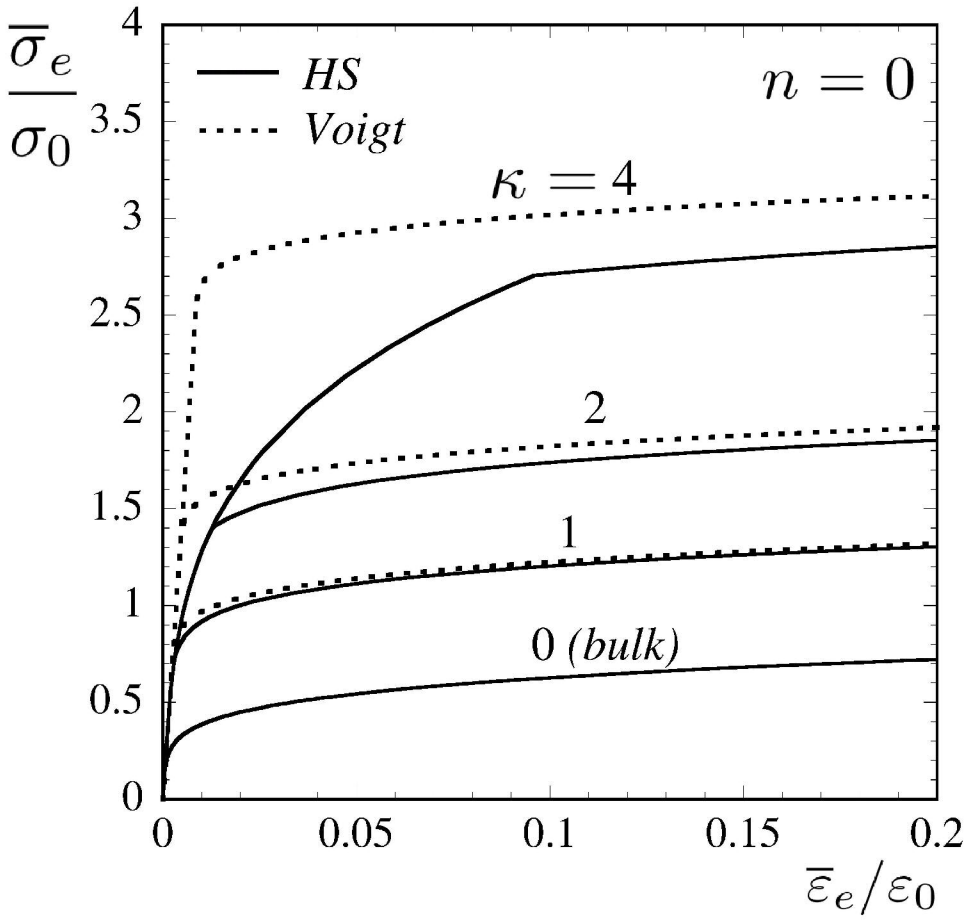


**3c**
164x151mm (600 x 600 DPI)

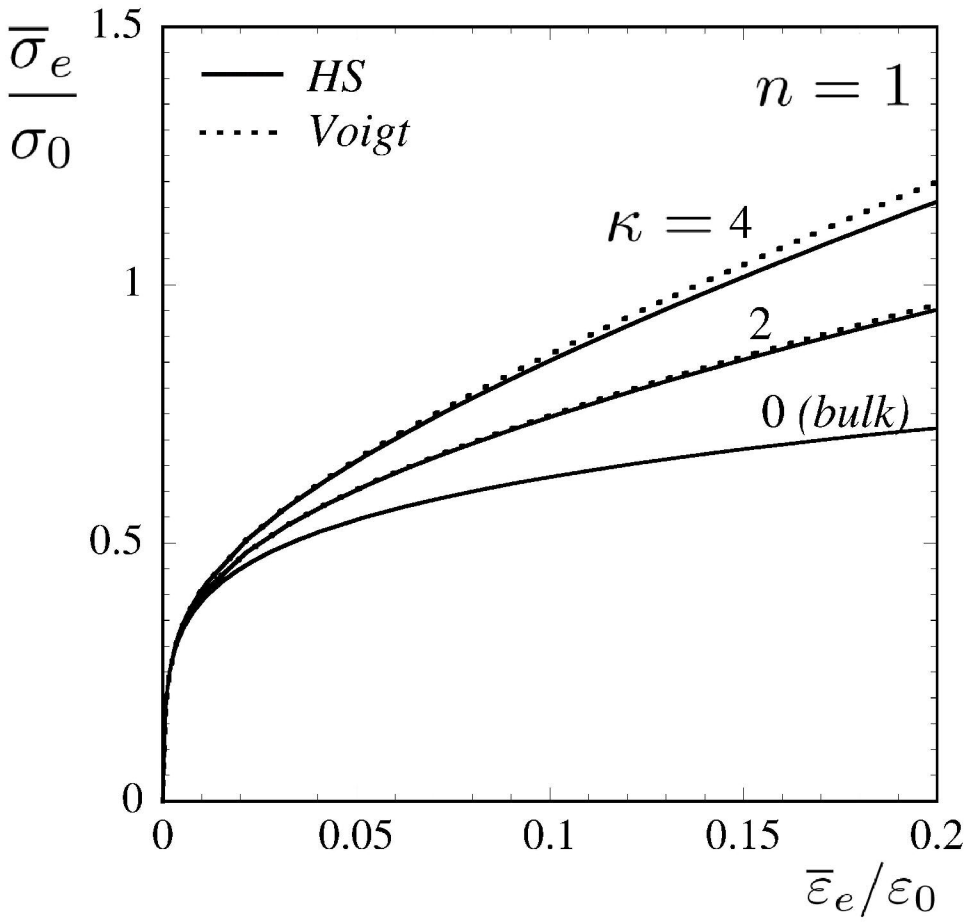


**3a**
164x151mm (600 x 600 DPI)

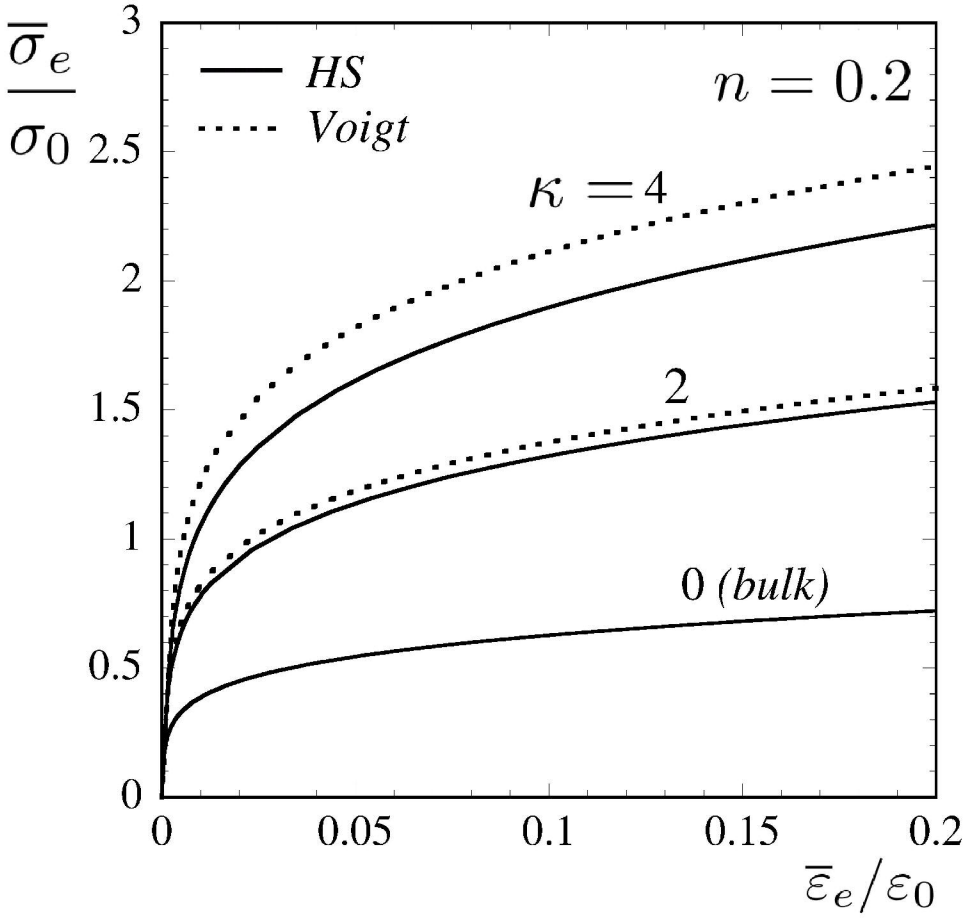


**3b**
164x151mm (600 x 600 DPI)

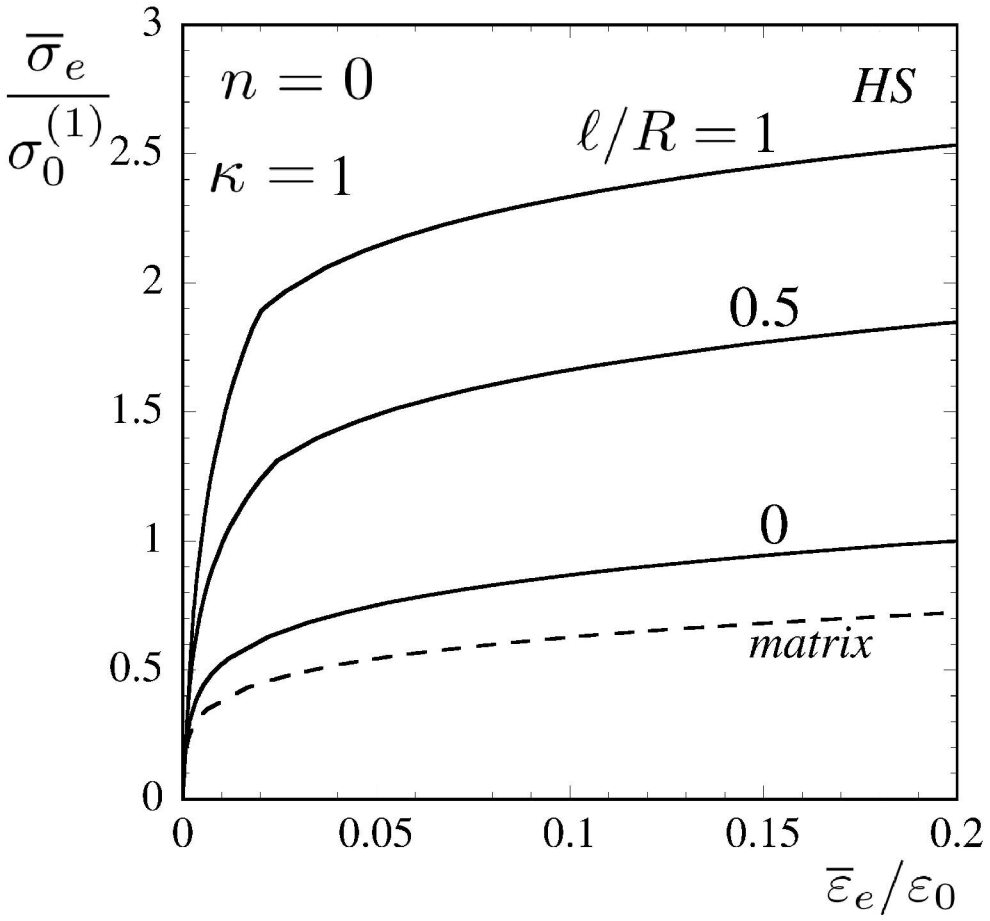


**4c**
164x151mm (600 x 600 DPI)

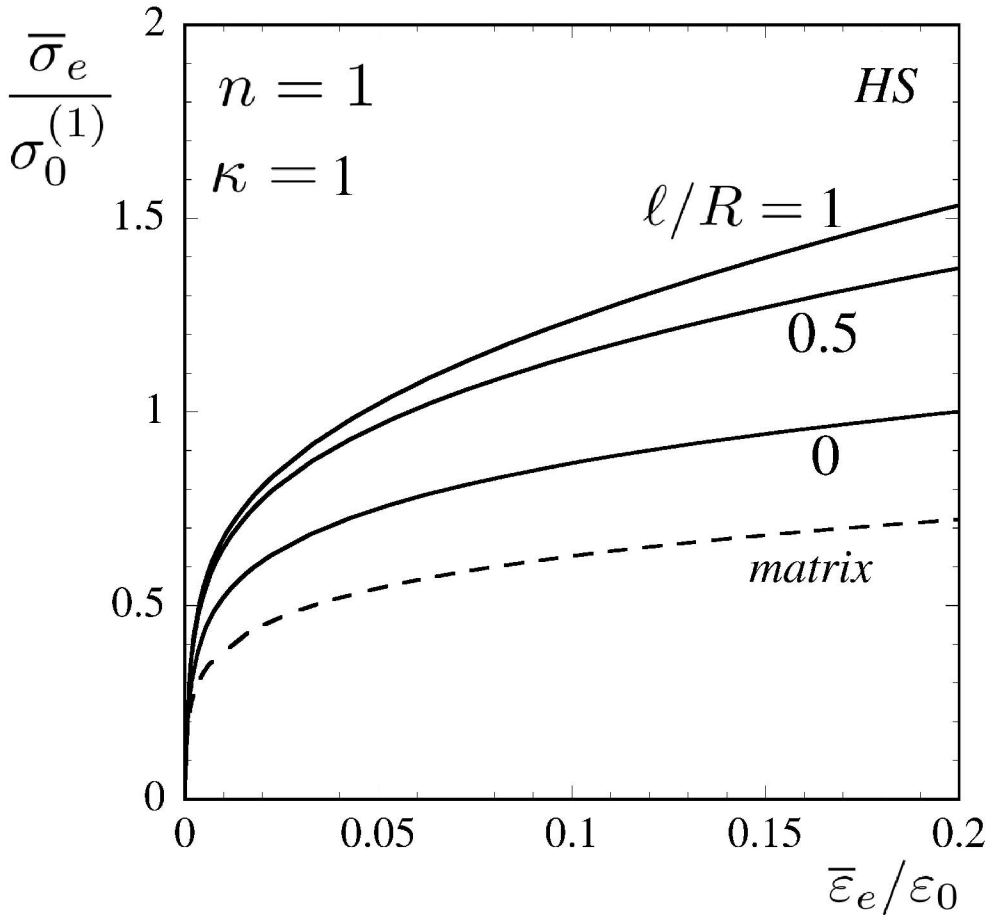


**4a**
164x151mm (600 x 600 DPI)

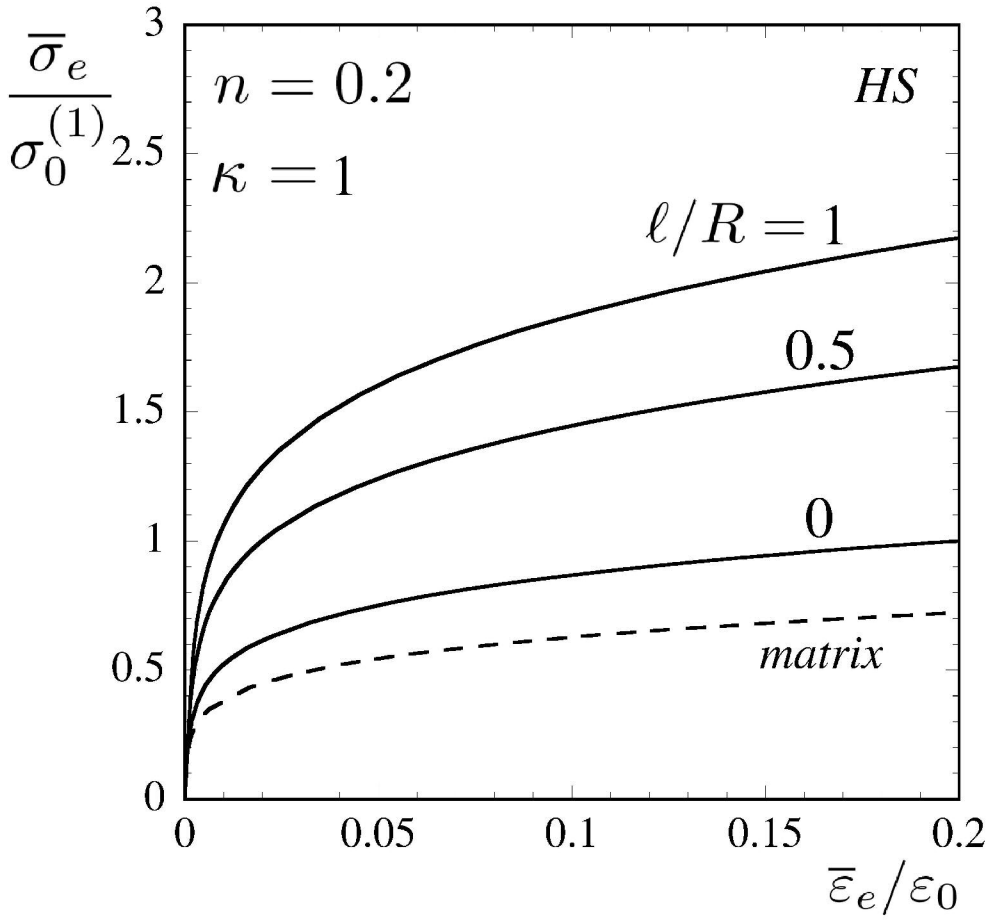


**4b**
164x151mm (600 x 600 DPI)